Seismic displacements of geosynthetic-reinforced soil modular block walls

C. C. Huang[1], L. H. Chou[2] and F. Tatsuoka[3]

[1]*Professor, Department of Civil Engineering, National Chi Nan University, No. 1, University Road, Puli, Nanton, Taiwan 545, Telephone: +886 49 2910960, Telefax: +886 49 2918679, E-mail: samhuang@ncnu.edu.tw*
[2]*Former graduate student, Department of Civil Engineering, National Chen Kung University, No. 1, Ta-Hsueh Road, Tainan, Taiwan 70101*
[3]*Professor, Department of Civil Engineering, University of Tokyo, 7-3-1, Hongo, Bunkyo-ku Tokyo, 113, Japan, Telephone: 81/3 3812 2111, Telefax: 81/3 5689 7268, E-mail: tatsuok@hongo.ecc.u-tokyo.ac.jp*

Received 30 May 2002, revised 28 March 2003, accepted 1 April 2003

ABSTRACT: Four geosynthetic-reinforced soil modular block (GRS-MB) retaining walls that behaved differently during the 1999 Taiwan Chi-Chi earthquake were investigated by field surveying and soil testing. Pseudo-static analyses based on the two-wedge failure mechanism were performed to investigate the seismic stability of such GRS-MB walls. The analyses considered the structural function of the stacked block facing and the contribution of reinforcement-facing connection strength to the seismic stability of GRS-MB retaining walls. It was found that the facing-reinforcement connection strength and the block–block shear resistance strongly affect the seismic stability and seismic displacement of GRS-MB retaining walls. Newmark's sliding block theory together with a 'displacement diagram' were used to evaluate the seismic displacements of the investigated walls. The displacement analyses give the values of horizontal seismic displacement of the discrete modular block facing and the vertical settlement of the backfill soil. It was found that the calculated values of wall displacements were comparable with the measured ones when the structural effects of the facing were properly accounted for. The effect of buckling mode deformation of the stacked blocks on the horizontal displacement of the GRS-MB walls is also evaluated quantitatively.

KEYWORDS: Geosynthetics, Failure, Geosynthetic-reinforced modular block wall, Pseudo-static analysis, Seismic displacement, Seismic stability

REFERENCE: Huang, C. C., Chou, L. H. & Tatsuoka, F. (2003). Seismic displacements of geosynthetic-reinforced soil modular block walls. *Geosynthetics International*, **10**, No. 1, 2–23

1. INTRODUCTION

The construction of geosynthetic-reinforced soil modular block (GRS-MB) retaining walls is relatively new in Taiwan. Therefore the first experience of GRS-MB retaining walls during a major earthquake was the Chi-Chi earthquake ($M_w = 7.7$ or $M_L = 7.3$), which occurred at 1:47 a.m. on 21 September 1999. This experience provided a valuable insight into the failure mechanism of GRS-MB retaining walls during major earthquakes, and thus an enhanced understanding of their seismic behaviour. This earthquake was triggered by a fracture of the Chelungpu Fault, which extends approximately in the N–S direction and dips at an angle of about 30° towards the east in central Taiwan (Figure 1). Huang (2000) reported results from a preliminary investigation into the behaviour of soil-retaining structures during this earthquake, showing the locations and performance of the two totally failed GRS-MB retaining walls. In addition to the two failed GRS-MBs reported by Huang (2000) (Figures 2 and 3), one lightly damaged and one undamaged GRS-MB (Figures 4 and 5) were investigated in the present study. The cross-sections of these walls after the earthquake are shown in Figures 6(a), 6(b), 7(a), 7(b), 11 and 12. The peak horizontal ground acceleration (a_{max}) recorded at sites 1–4 where these walls were located is approximately 450 gal (acceleration due to gravity = 980 gal).

In the seismic design method for GRS-MB retaining walls proposed by Bathurst *et al.* (1997), the Mononobe–Okabe (M-O) pseudo-static earth pressure theory (Mononobe 1924; Okabe 1924) is used to evaluate the internal and external stability of walls after some modifications to the distribution of the dynamic component of earth pressure. The seismic design guidelines (Bathurst 1998) are based on the aforementioned method, suggesting that, for GRS-MB retaining walls to be constructed in the seismically active area where values

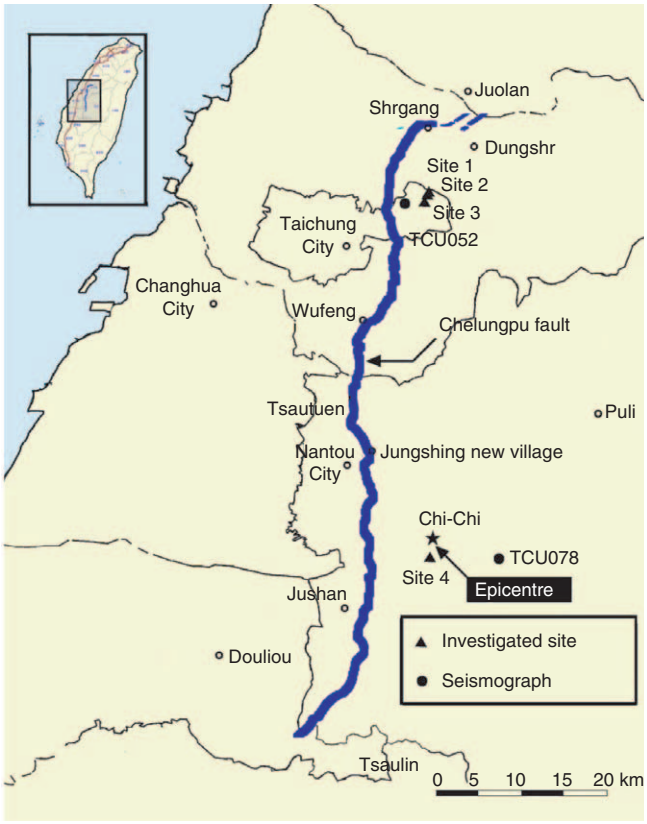

Figure 1. Locations of the surface scarp induced by the fracture of the Chelungpu fault during the 1999 Taiwan Chi-Chi earthquake

Figure 2. Collapsed GRS-MB wall at site 1

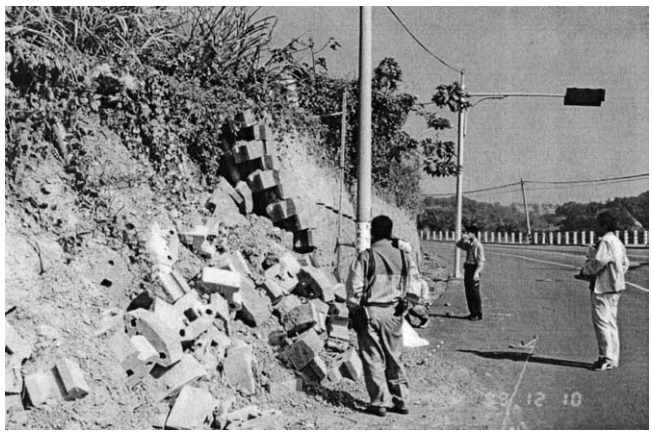

Figure 3. Collapsed GRS-MB wall at site 2

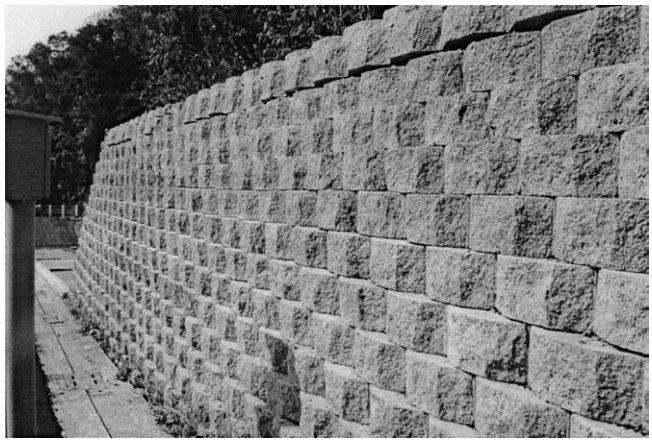

Figure 4. Lightly damaged GRS-MB wall at site 3

Figure 5. Undamaged GRS-MB wall at site 4

of a_{max} higher than $0.4g$ are anticipated (g is the acceleration due to gravity = 980 gal), the residual displacement and deformation of the wall should be evaluated. After the 1995 Hyogo-ken Nambu earthquake, the Japanese Railway Technical Research Institute (JRTRI) developed a displacement-based seismic design method for reinforced and unreinforced railway embankments subjected to major earthquakes (so-called Level 2 design earthquakes; JRTRI, 1999), which was later approved by the Japanese Ministry of Transport. In this method, the seismic residual displacement of an embankment is evaluated by Newmark's sliding block theory (Newmark 1965), based on pseudo-static limit equilibrium stability analysis assuming a circular potential failure surface. The introduction of displacement-based seismic design of GRS-MB retaining walls is intended to obtain more cost-effective and/or practical wall geometries.

Nevertheless, the existing design methods for seismic stability of GRS-MB retaining walls are not sufficient, and need to be modified to explain the behaviour of the GRS-MB retaining walls during the 1999 Chi-Chi earthquake, including two totally failed walls. This is

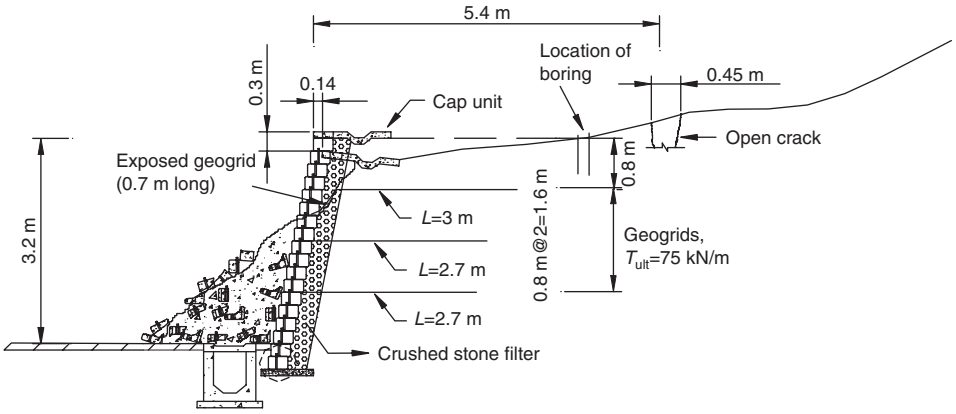

Figure 6(a). Cross-section of the failed GRS-MB wall at site 1

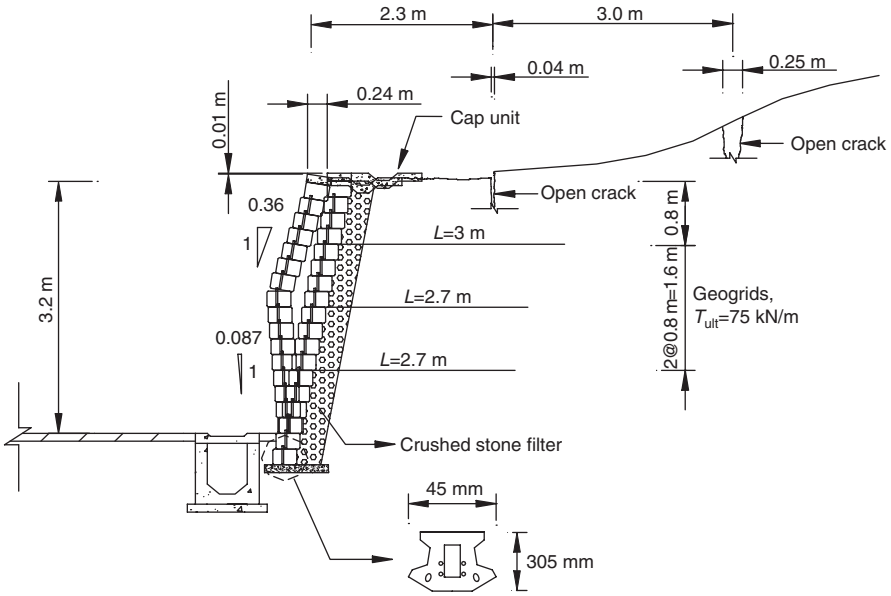

Figure 6(b). Severely deformed section of the GRS-MB wall adjacent to the failed wall at site 1

because the failure of the GRS-MB retaining walls was seemingly triggered by failure of the modular block facing as a result of insufficient connection strength, and also by excessive buckling-mode deformation. These failure modes are not adequately accounted for in the existing design methods, as discussed by Huang *et al.* (2001).

In view of the above, a pseudo-static limit equilibrium-based stability analysis method that has been proposed by Huang *et al.* (2001) was extended. This method was validated through analysis of the case histories of the failed, lightly damaged and undamaged GRS-MB retaining walls during the 1999 Chi-Chi earthquake.

2. LITERATURE REVIEW

Numerical analyses, such as finite element methods (FEM) and finite difference methods (FDM), are often performed to evaluate the displacement and deformation of soil structures to overcome the inherent limitations of limit-equilibrium stability analysis. Encouraging results with respect to the seismic displacement and deformation of GRS retaining walls obtained using numerical analyses have been reported by Bathurst and Hatami (1998), Bathurst *et al.* (1997) and Carotti and Rimoldi (1998). For soil structures exhibiting large displacements and significant strain localisation in shear bands in the soils, full considerations of factors such as shear banding, strain-softening and anisotropy in the FEM analysis may give encouraging results, as demonstrated for the bearing capacity problem of footings on unreinforced and reinforced sand by Siddiquee *et al.* (1999) and Kotake *et al.* (2001). However, this is too complicated to use in ordinary design practice. More detailed discussion of this issue is beyond the scope of the present study.

Newmark's sliding block theory is often used to evaluate relatively large displacements of GRS retaining walls. In such an analysis, buckling failure of the discrete block (or panel) facing, as observed by Tatsuoka (1993) and also in the prototype cases analysed in the present study (Figures 6b and 7b), is one of the possible failure modes of reinforced soil-retaining walls. However, this failure mode was not accounted for, or not successfully

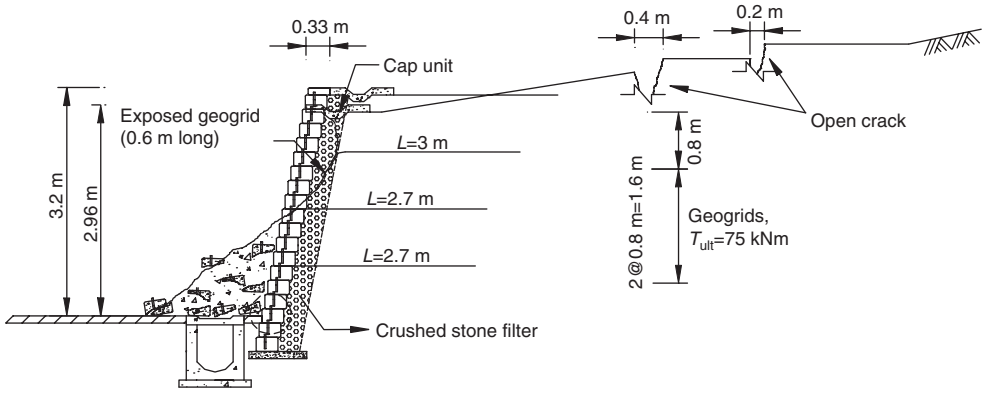

Figure 7(a). Cross-section of failed GRS-MB wall and a nearby failed cantilever wall at site 2

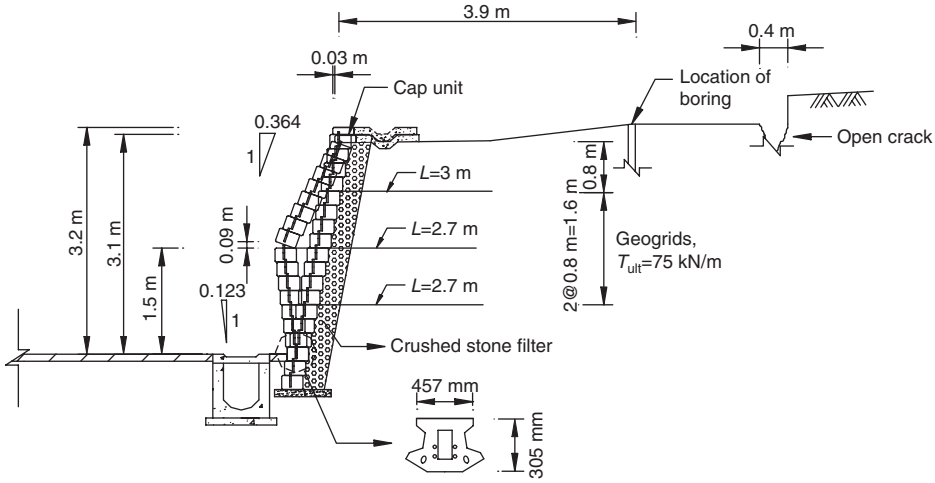

Figure 7(b). Severely deformed section of the GRS-MB wall adjacent to the failed wall at site 2

predicted, in the previous analyses in the literature. For example, Cai and Bathurst (1996) performed a parametric study on a 6-m-high GRS-MB retaining wall based on Newmark's theory for prescribed displacement modes (horizontal sliding along a reinforcement–soil interface and/or along a block–block interface). However, it is not certain that the assumption of the horizontal sliding mode as the critical failure mode was realistic, or whether the calculated wall displacement mode was consistent with the observed one. Ling and Leshchinsky (1998) also used Newmark's sliding block theory to analyse the displacement of a GRS retaining wall with a cast-in-place full-height rigid facing (the so-called Tanata wall) that was subjected to strong seismic loading during the 1995 Hyogo-ken Nambu earthquake (Tatsuoka *et al*. 1998). The Tanata wall was constructed using a GRS retaining wall technology called the 'reinforced railway embankment with rigid facing (RRR) method' (Tatsuoka 1993; Tatsuoka *et al*. 1997). In their analysis, horizontal sliding of the reinforced soil zone along the horizontal interface between the reinforced backfill zone and the subsoil was assumed. However, it seems that this assumed failure mode is not truly representative of the actual failure mode, which includes a large component of tilting.

Summarising the above, it seems that the following three main limitations need to be overcome to apply Newmark's method to more general cases, including the case histories of the four GRS-MB retaining walls analysed in the present study:

1. The critical failure mechanism assumed in most of the existing seismic design methods for GRS retaining walls is Coulomb's triangular failure wedge, as used for conventional soil-retaining walls with unreinforced backfill (e.g. Bathurst *et al*. 1997). The bi-linear (or two-wedge) failure mechanism has long been used in the routine design of reinforced steep slopes and reinforced retaining walls (e.g. Horii *et al*. 1994; Jewell *et al*. 1984; Tatsuoka and Yamauchi 1986; Tatsuoka *et al*. 1998). The results from model tests in the laboratory and full-scale static loading tests (Tatsuoka *et al*. 1989, 2000) have also shown that the bi-linear (or two-wedge) failure mechanism is the critical failure mechanism of GRS retaining walls. This is also true for model shaking table tests on GRS retaining walls. Matsuo *et al*. (1998) performed a series of shaking table tests on 1-m-high models of GRS retaining walls using various types of reinforcement and facing. The backfill was medium-dense air-dried Toyoura sand with a relative density of about 60%. Both sinusoidal and irregular time histories of base acceleration, with the maximum acceleration ranging between 54 gal and 575 gal, were applied at

the shaking table. In tests on models of typical GRS retaining walls having a discrete panel facing with a reinforcement length of 0.7 times the wall height (= 1.0 m) and a vertical spacing of reinforcement of 200 mm, the failure surface was bi-linear as represented by the so-called 'two-wedge' failure mechanism. The two-wedge failure mechanism was also observed in a series of model shaking table tests on GRS retaining walls with a full-height rigid facing (RRR walls: see Koseki *et al.* 1997, Tatsuoka *et al.* 1998).

2. Tatsuoka *et al.* (1989, 1993, 1997, 2000) and Tatsuoka (1993) pointed out the importance of the structural role of the facing for the seismic stability of GRS retaining walls, based on the results of static and dynamic loading tests on small models and static loading tests on full-scale GRS reinforced retaining walls. The importance of the bending and shear resistance of the facing for the seismic stability of GRS retaining walls was also confirmed by Bathurst *et al.* (1997) by performing shaking table tests on reinforced model walls having various types of facing with different connection conditions. Nevertheless, the contribution of the bending and/or shear resistance of the facing to the seismic stability of GRS retaining walls has yet to be taken into account in many of the existing seismic design guidelines and specifications.
3. The existing seismic displacement calculation methods for GRS retaining walls are based on the pseudo-static approach (e.g. Cai and Bathurst 1996; Ling and Leshchinsky 1998), assuming that the reinforced backfill zone together with the facing behaves as a rigid mass during earthquakes. As a result, only horizontal sliding at the interface between the reinforced backfill (including the facing) and the subsoil becomes kinematically admissible. This failure mode may be not appropriate in many actual cases, including the four case histories that are analysed in the present study. In particular, such a horizontal sliding mode becomes unrealistic when the facing is embedded to some depth in the subsoil and a large passive earth pressure can be activated on the front face of the embedded part of the facing, as typically shown in Figure 6b. Matsuo *et al.* (1998) also observed the greatest displacement at the mid-height of the discrete panel facing in their shaking table tests.

The present study strives to eliminate the above-mentioned limitations in the existing seismic design methods for GRS retaining walls, including GRS-MB retaining walls. A method that has been developed by Huang *et al.* (2001) for examining the deformation and displacement of a GRS-MB retaining wall at site 1 is extended and validated. This method uses the two-wedge failure mechanism in the stability analysis while accounting for the interaction and displacement compatibility between the soil wedges and the facing structure.

3. SITE INVESTIGATION

At sites 1 and 2, two 3.2-m-high GRS-MB retaining walls collapsed in similar modes. Typical collapsed and greatly deformed sections of the damaged walls at sites 1 and 2 are shown in Figures 6a, 6b, 7a and 7b. These two walls were constructed at the same time in 1999 by the same contractor as a rock fall mitigation zone at the upper side of the 40-m-wide highway. The backfill was loosely compacted soil. Reinforced concrete (RC) cantilever retaining walls that had been constructed as the major soil-retaining facilities at the opposite side of the highway in the highway-widening project were intact (see Figure 14). A settlement of only 50–200 mm was detected on the pavement on the back of the nearby RC retaining wall, and hardly any tilting was visible with the RC walls. At the sections of the GRS-MB retaining walls that were on the verge of total collapse (Figures 6b and 7b), the facing bulged between the lower third and half of the wall height, exhibiting large openings between vertically adjacent modular blocks. As mentioned above, this failure mode is similar to that observed by Matsuo *et al.* (1998) in a series of shaking table tests on reinforced soil-retaining wall models with a discrete panel facing. It is also important to note that a full rupture took place at the junctions between the longitudinal and transverse members of the geogrid at the connections between the geogrid and the collapsed modular block facing at sites 1 and 2 (Figure 8). The locations of the failed junctions coincided with those of the FRP connecting pins (15 mm in diameter and 200 mm long; Figure 9) used to restrain relative lateral displacements between vertically adjacent modular blocks. The reinforcement was a knitted polyester geogrid (that is, a PET geogrid), which had an ultimate tensile strength (T_{ult}) of 75 kN/m in the longitudinal direction and a low junction strength of 0.3 kN/junction, both measured at an extension rate of 10%/min. In addition, it seems that the connection pins were too short to ensure the integrity of the facing by restraining the bulging of the facing induced by large earth pressure at

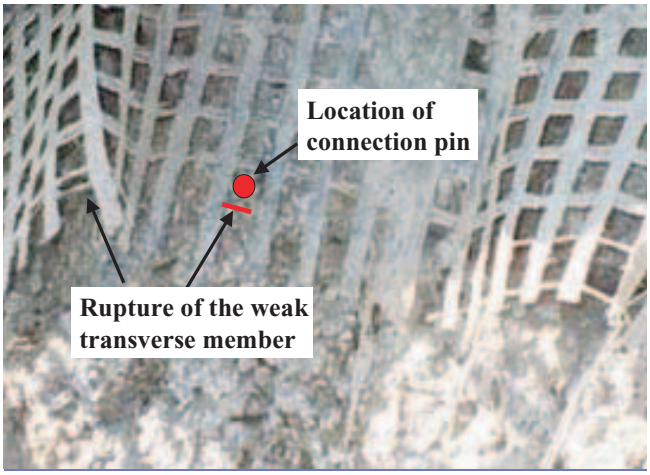

Figure 8. Typical example of rupture at junctions of geogrid (sites 1 and 2)

Figure 9. Typical example of connection pin seen in an opening between modular blocks (sites 1 and 2)

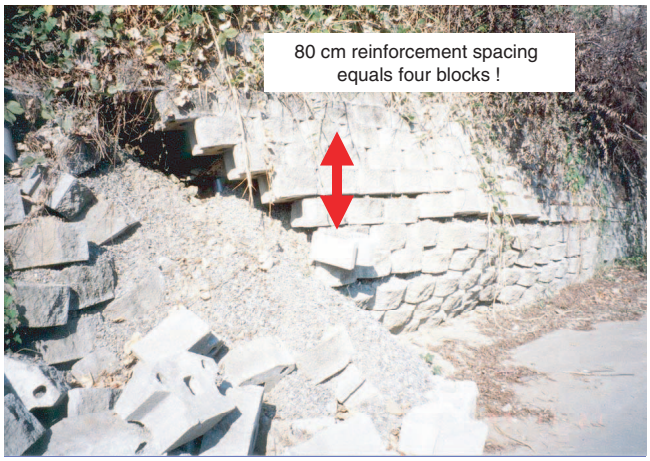

Figure 10. Typical example of failed GRS-MB retaining wall (sites 1 and 2)

the back of the facing during earthquakes (Figure 9). Furthermore, it seems that too large a vertical spacing between vertically adjacent reinforcement layers of 800 mm, encompassing four modular blocks, was another reason why the facing lost its integrity, exhibiting severe bulging or total collapse (Figure 10).

It seems from the above that the design of these failed walls: (i) underestimated the earth pressure acting on the back of facing; or (ii) assumed relevant seismic earth pressure but grossly overestimated the connection strength between the facing and the reinforcement; or (iii) assumed no buckling-like deformation of the block facing.

A lightly damaged 2.6-m-high GRS-MB retaining wall (Figures 4 and 11) was located at site 3, which was about 2 km south from sites 1 and 2 along the same highway. Only some minor cracks at the crest of the wall and slight displacement of the top layer of the modular block facing were found. The reinforcement used with the wall at site 3 is a woven PET geogrid that has similar T_{ult} and stiffness values as the knitted product used with the walls at sites 1 and 2, except that its junction strength is significantly lower. Although the blow counts obtained by standard penetration tests (N-values) at site 3 (Figure 15) are not greatly different from those obtained at sites 1 and 2 (Figures 13 and 14), there are some different conditions between the sites. The wall at site 3 is slightly shorter than those at sites 1 and 2. Also, a gravity soil-retaining wall was located behind the GRS-MB soil-retaining wall at site 3. The seismic behaviour of the GRS-MB retaining wall might have been influenced by that of the gravity wall.

An intact 5.4-m-high GRS-MB retaining wall (Figures 5 and 12) was located at site 4, which was about 5 km south of the epicentre in Chi-Chi township (see Figure 1). This wall had been constructed to support a parking lot along an access road to a new bridge. Most of the piers of this bridge were moderately damaged during the

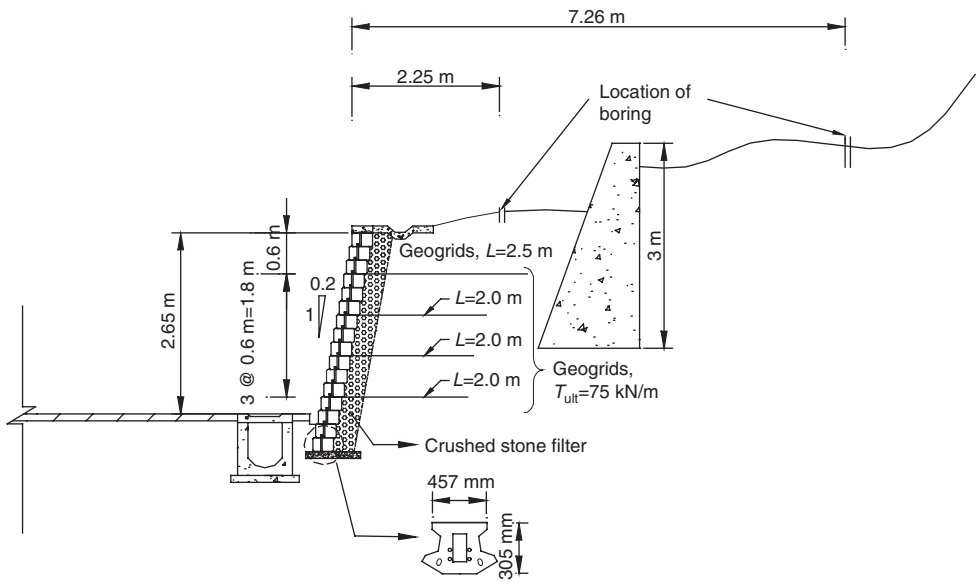

Figure 11. Cross-section of lightly damaged (or intact) GRS-MB at site 3

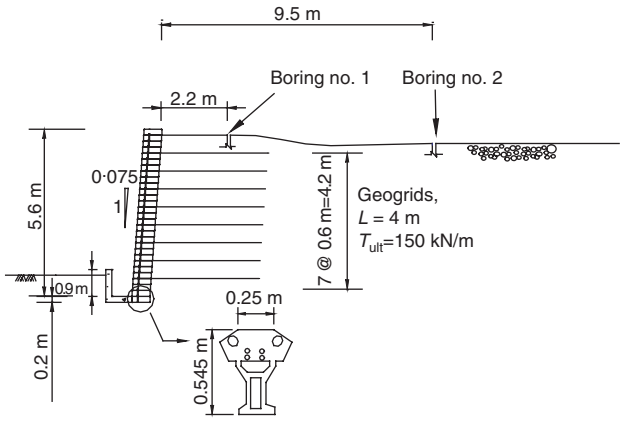

Figure 12. Cross-section of intact GRS-MB at site 4

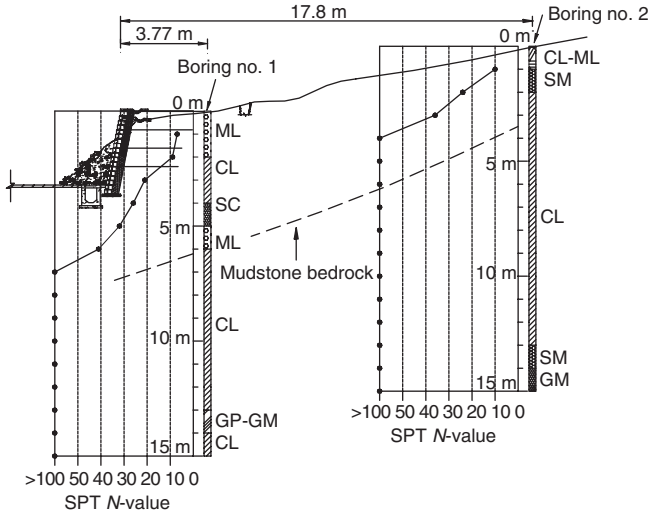

Figure 13. Soil profiles, *N*-values and soil classification at site 1

earthquake, and were reinforced using steel plate in the post-earthquake retrofit work. Although the GRS-MB retaining wall at site 4 was the highest of those investigated in the present study, it showed no visible tilting, displacement or deformation, nor cracking on its facing and crest. The different conditions between the wall at site 4 and those at sites 1, 2 and 3 include the following:

- Larger modular blocks were used as the facing elements at site 4 (see Figure 12).
- The backfill of the GRS-MB retaining wall at site 4 was a well-compacted gravel, in contrast to the sandy or silty soils with smaller particle sizes used at sites 1, 2 and 3. In fact the *N*-values measured in the backfill at site 4 were very high ($N > 100$; see Figure 16), indicating that it was stronger and stiffer than the backfill at sites 1, 2 and 3.
- Although the reinforcement used at site 4 is a woven PET geogrid, like that used at site 3, its tensile strength (T_{ult}) was 150 kN/m, which is higher by a factor of two than that of the reinforcement used at sites 1, 2 and 3 ($T_{ult} = 75$ kN/m). This geogrid also had a junction strength as low as that of the geogrid used at site 3.

The internal friction angles, ϕ_s, of the backfill of the walls at sites 1–4 were evaluated by direct shear tests on specimens reconstituted by compacting the backfill material from the respective sites to achieve the measured values of field dry density and water content. These values, which are summarised in Table 1, were used in the analysis shown below. In the present analysis, the peak friction angle of the backfill, ϕ_s, rather than the residual friction angle, ϕ_{res}, was used, for the following reasons:

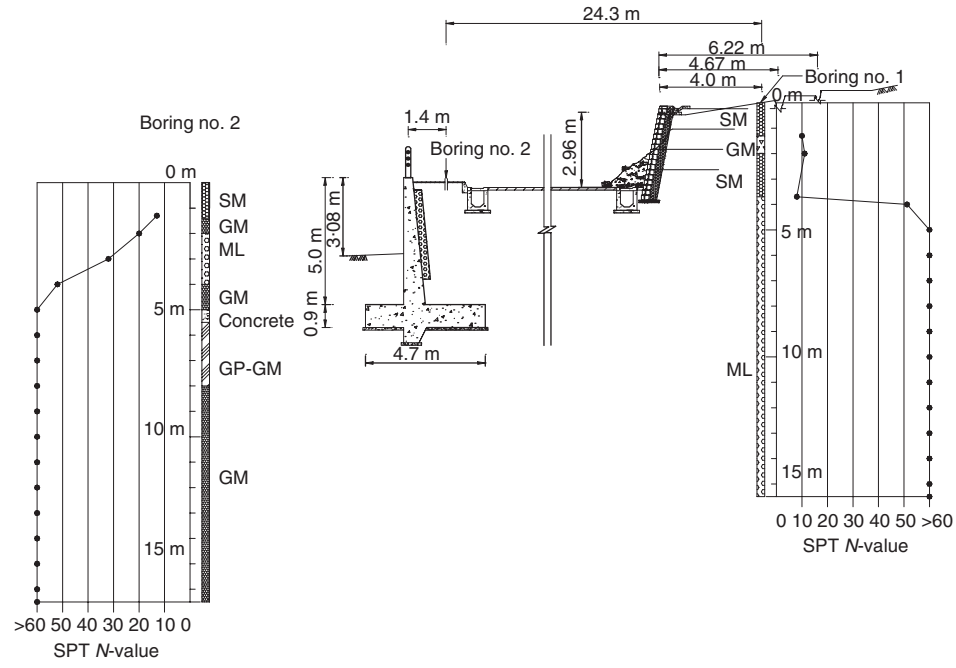

Figure 14. Soil profiles, *N*-values and soil classification at site 2

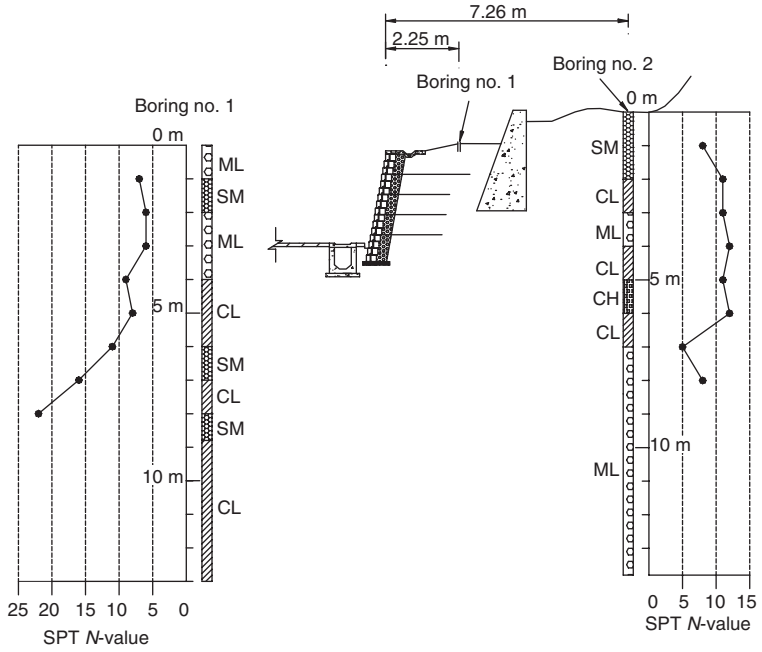

Figure 15. Soil profiles, *N*-values and soil classification at site 3

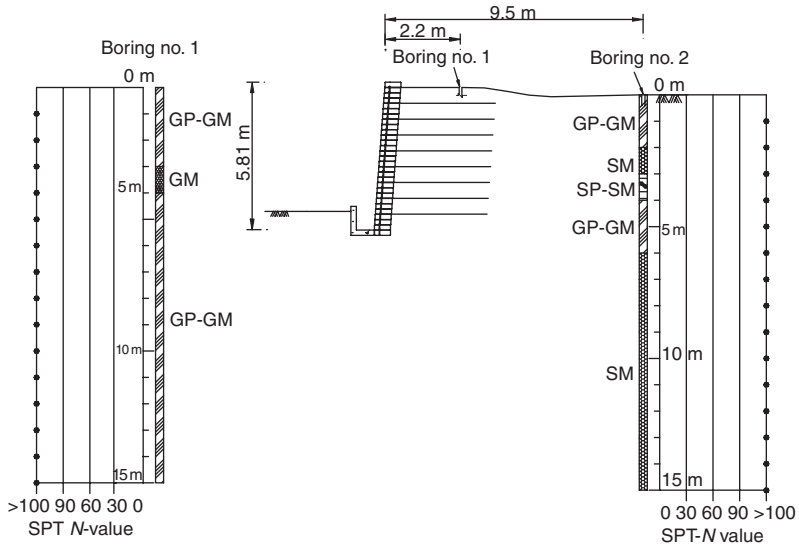

Figure 16. Soil logs and *N*-values obtained at site 4

Table 1. Properties and strength parameters of backfill soil at sites 1–4

	Site 1	Site 2	Site 3	Site 4
Unified soil classification	ML, CL	SM, GM	SM, ML	GP-GM, GM
Unit weight (kN/m^3)	21.3[(a)]	19.1[(a)]	18.9[(b)]	22.7[(b)]
Water content (%)	16.5[(a)]	12.1[(a)]	12.1[(b)]	3.9[(b)]
Cohesion (kPa)	0	0	0	0
Friction angle (°)	29.2–30.4[(c)]	29.2–30.4[(c)]	33.6–34.8[(c)]	48.1–49.8[(d)]
SPT N-values	8–10	~10	6–7	≥100
ϕ_s estimated from *N*-values[(e)] (°)	25–36	26–36	23–34	49

[(a)] Measured by the in-situ sand cone method.
[(b)] Obtained using samples retrieved from the respective boring hole.
[(c)] The range indicates friction angles obtained from direct shear tests using small-size (63 mm dia. × 42 mm) and large (200 mm dia. × 113 mm) specimens.
[(d)] Obtained from direct shear tests using large specimens.
[(e)] According to Dunham's empirical equations $\phi = \sqrt{12N} + 15^\circ$ and $\phi = \sqrt{12N} + 25^\circ$ (Japanese Geotechnical Society 1988).

- The backfill of the damaged walls at sites 1, 2 and 3 was relatively loose. Therefore the residual state was not attained in the direct shear tests of the backfill soil.
- The use of a single value of peak friction angle, ϕ_s, obtained by a certain type of element test in limit-equilibrium stability analysis, as in the present study, is already an approximation to the friction angles actually mobilised along the failure planes at the moment of failure of the soil mass concerned. This is because the peak strength of the backfill soil is never mobilised simultaneously along the failure plane, owing to the progressive nature of failure. In addition, inherent anisotropy may have significant effects on the peak strength. It is not a simple task to take these factors into account in limit-equilibrium stability analysis.

4. MODIFIED TWO-WEDGE METHOD

Figure 17 shows the force system used in the modified two-wedge analysis proposed in the present study. The potential failure lines consist of three parts: a bi-linear segment in the backfill, a linear vertical segment along the block–block interface of soil wedges B and F, and a linear inclined segment along the interface between wedge F and the facing. The safety factor against shear failure along the potential failure lines is defined as:

$$F_s = \frac{\tau_f}{\tau_m} \tag{1}$$

in which τ_f is the ultimate shear strength of the backfill soil, based on the Mohr–Coulomb failure criterion:

$$\tau_f = c_s + \sigma_n \tan \phi_s \tag{2}$$

where c_s and ϕ_s are the cohesion intercept and internal friction angle of the backfill soil, and σ_n and τ_m are the normal and shear stresses acting on the failure plane in the backfill. In the analysis of the case histories performed in the present study, the inter-wedge friction angle, ϕ_{BF}, and the cohesion intersect, c_{BF}, were taken as zero to simulate the large displacements and open cracks observed at sites 1 and 2. On the other hand, it was assumed that, when the connection strength of the reinforcement at the back of the facing is taken into account, the friction angle at the interface between the back of the facing and the backfill, ϕ_{FW}, is equal to ϕ_s, whereas the cohesion intersect, $c_{FW} = c_s = 0$, by considering that the rear side of the modular blocks is very rough, and a gravelly filter layer has been placed behind the modular block facing. This definition of safety factor (Equation 1) is consistent with the one that has been used for decades in conventional slope stability analysis. The formulations and computer algorithm that were used to obtain the safety factor, F_s, and the critical failure mechanism under seismic loading conditions are summarised in Appendix A.

A specific feature of the modified two-wedge method proposed in this paper is that, to overcome limitation 2 discussed above, the structural effects of the facing on the stability of the whole soil-retaining wall system were taken into account quantitatively when evaluating the potential shear failure along the composite potential failure planes. This objective was achieved by searching for the mobilised material strengths—that is, the factored strengths equal to c_s/F_s, $\tan \phi_s/F_s$ or $(c_s + \tan \phi_s)/F_s$—for every segment of the failure planes by iterative calculations ascertaining the force equilibrium in both the horizontal and vertical directions of wedges B and F and the facing. The concept of hinge height as suggested by the NCMA (Collin 1996) was used to evaluate the maximum height of modular blocks that provides effective normal pressure at the bottom of the stacked blocks. According to this concept, the effective heights for providing overburden of the

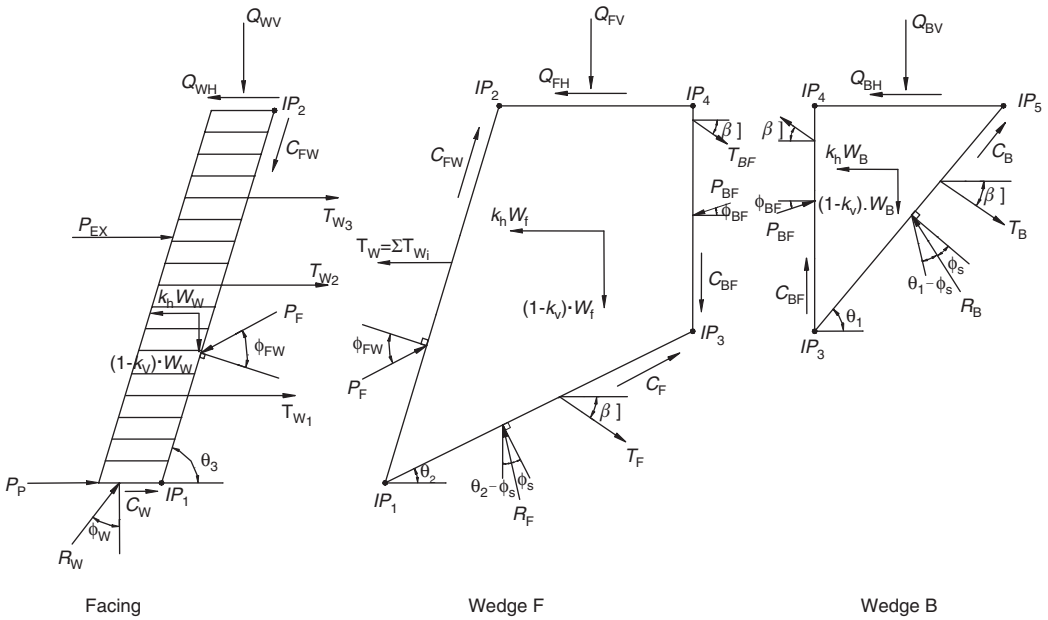

Figure 17. Force equilibrium in the modified two-wedge method

modular block facing are equal to 0.77 m for the walls at sites 1–3 and 6.5 m for the wall at site 4. The significantly larger value for the wall at site 4 is due to its steeper facing slope and its larger modular blocks, as shown in Figure 12.

5. VALIDATION OF THE PROPOSED METHOD

In the present study, the horizontal pseudo-static seismic coefficient, k_h, and the ratio of the vertical component, k_v, to k_h, λ ($= k_v/k_h$), were used as input parameters, instead of k_h and k_v. Representative values of λ for the ground acceleration during the Chi-Chi earthquake at the sites of the GRS-MB retaining walls were calculated based on the composite acceleration of the NS and UD components recorded at two nearby seismographs (TCU052 and TCU078). For the major pulses in the NS direction with a horizontal ground acceleration larger than 200 gal, the measured value of λ was approximately equal to 0.2. Therefore the value $\lambda = 0.2$ was used throughout the present study.

Figure 18 compares the seismic earth pressure coefficient, $K_{AE,}$ for a hypothetical configuration of a conventional retaining wall with unreinforced backfill calculated by the following three methods:

- the two-wedge method proposed in this paper under the conditions $\phi_{BF} = 0$ or $\phi_{BF} = \phi_s$;
- the Mononobe–Okabe (M-O) method (assuming triangular wedge failure mechanism); and
- the two-wedge method by Jewell *et al.* (1984).

In the present analysis, the two-wedge failure mechanism was dominant when $\phi_{BF} = 0$, whereas the one-wedge (i.e. $\theta_1 = \theta_2$) failure mechanism was dominant when $\phi_{BF} = \phi_s$. It can be seen that the seismic earth pressure acting on the back of the retaining wall structure obtained under the condition $\phi_{BF} = \phi_s$ compares well with those obtained by the M-O method, whereas the value obtained under the conditions $k_h = 0$, $\phi_{BF} = 0$ and $\phi_{FW} = \phi_s/2$ compares well with that obtained using the two-wedge method by Jewell *et al.* (1984) under the conditions $k_h = 0$, $\phi_{BF} = 0$ and $\phi_{FW} = 0$. The results of a parametric study on the M-O seismic earth pressure coefficient showed that the effect of ϕ_{FW} ($= 0°$ and $20°$) on the values of K_{AE} is small.

It can also be seen that the seismic earth pressure obtained for the condition $\phi_{BF} = 0$ is consistently greater than the value when $\phi_{BF} = \phi_s$, indicating that the use of the seismic earth pressure acting on the wall obtained by the present analysis method may be slightly conservative when used in design.

6. MODELLING OF STRUCTURAL EFFECTS OF FACING AND CONNECTION STRENGTH

Figure 19 shows schematically the reinforcement force developed at various locations of each reinforcement layer. To investigate the structural effects of the facing, and the effects of the connection strength between the facing and the reinforcement, on the seismic stability of GRS-MB retaining walls, the following three types of analysis with different combinations of facing structural feature and connection strength as summarised in Table 2, were investigated.

6.1. Type 1 analysis

In this analysis, neither the structural strength of the facing nor the connection strength were considered, which is equivalent to the conventional two-wedge analysis. The mobilised tensile force, T_s, in the reinforce-

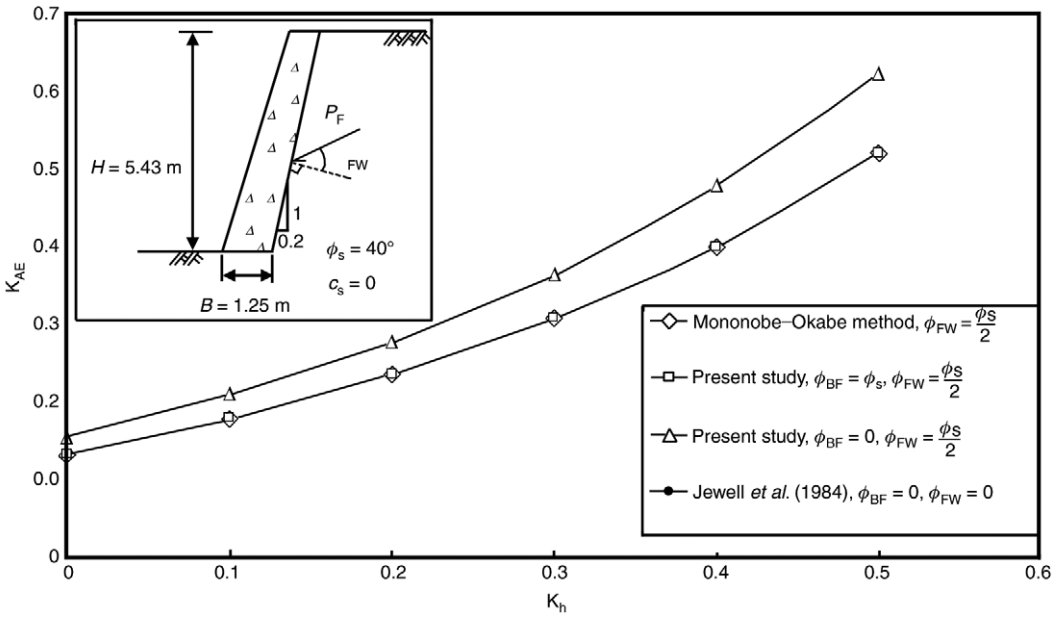

Figure 18. Comparison of seismic lateral force against wall obtained using various methods

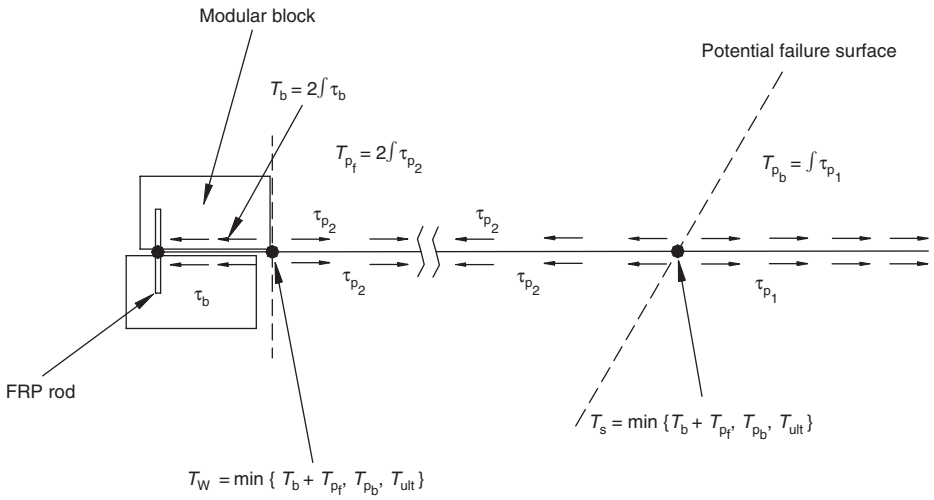

Figure 19. Schematic figure for calculating connection force and reinforcement force acting on potential failure surface

Table 2. Three types of analysis for different combinations of facing structural feature and connection strength

	Structural strength of facing	Connection strength, T_{w_i}	Shear strength of FRP connection pins
Type 1	No	No	No
Type 2	Yes	Yes	No
Type 3	Yes	Yes	Yes

ment at the failure plane is therefore equal to the smallest one among three different quantities as:

$$T_s = \min\{T_{p_b}, T_{p_f}, T_{ult}\} \quad (3)$$

where T_{p_b} is the resistance of the reinforcement to pull-out from the backfill zone behind the potential slip surface, T_{p_f} is the resistance of the reinforcement to pull-out from the backfill zone in front of the potential slip surface, and T_{ult} is the tensile rupture strength of the reinforcement. The tensile force T_s becomes zero when the failure plane coincides with the interface between the back of the facing and the backfill.

6.2. Type 2 analysis

In this analysis, the structural strength of the facing was taken into account without considering any contribution of the strength of the connection pins placed between vertically adjacent facing blocks to the limit equilibrium stability along the critical failure planes. The pull-out resistance, T_b, of the geogrid from the interface between the vertically adjacent blocks of the facing was taken into account. The mobilised tensile force, T_s, in the reinforcement at the failure plane is therefore determined as

$$T_s = \min\{T_b + T_{p_f}, T_{p_b}, T_{ult}\} \quad (4)$$

where the term T_{p_f} in Equation 3 has been replaced by the term $T_b + T_{p_f}$, where T_b is the pull-out resistance of geogrid, which is the sum of the shear resistance at the interface between the vertically adjacent blocks and the junction strength, T_j, of the geogrid at the connection pins. By denoting T_b as

$$T_b = 2\int \tau_b, \quad \tau_b = C_{b\text{-}r} + P_n \cdot \tan\phi_{b\text{-}r}$$

we mean the equivalent bond strength at the interface between the reinforcement and the facing blocks including the junction strength of the geogrid, T_j. In the present study, an apparent cohesion $C_{b\text{-}r} = 7.8$ kN/m and a friction angle $\phi_{b\text{-}r} = 21^\circ$ were evaluated by pull-out tests using similar types of reinforcement and facing blocks (University of Wisconsin-Platteville, 1993). For example, the value of T_b obtained by using these values of $c_{b\text{-}r}$ and $\phi_{b\text{-}r}$ at a normal stress, σ_n, of 30 kN/m^2 (equivalent to an overburden pressure at the block–block interface at a depth of about 1.5 m, $P_n = 30$ kN/m$^2 \times B$, $B = 0.305$ m) is equal to 11.3 kN/m. Bathurst and Simac (1997) reported a ratio of $T_b/T_{ult} = 0.13$–0.20 from a pull-out test using a woven polyester geogrid and hollow masonry concrete blocks with granular infill. By substituting $T_{ult} = 75$ kN/m, which was found to be relevant to the cases at sites 1–3, into $T_b/T_{ult} = 0.22$, we obtain a pull-out strength of $T_b = 10$–15 kN/m, which is comparable to the value used in the present study.

Unlike the type 1 analysis (Section 6.1), the mobilised connection force at the rear of the facing T_w is not equal to zero, but determined as

$$T_w = \min\{T_b, T_{p_b}, T_{ult}\} \quad (5)$$

It was assumed in the present analysis that, in examining the overall limit equilibrium along the failure planes, the friction angle at the block–block interface, ϕ_B, is equal to the friction angle of the backfill, ϕ_s, whereas the cohesion

intercept at the block–block interface, c_B, is equal to zero. Note that the use of $\phi_B = 30.4^\circ$ for sites 1 and 2 and $\phi_B = 34.8^\circ$ for site 3 is comparable to the results from the direct shear tests reported by Bathurst and Simac (1997): that is, they showed that, with hollow masonry block units with uniform crushed stone infill and connection pins, $\phi_B = 26^\circ - 35^\circ$ and $C_B = 5$–15 kN/m. The assumption of $C_B = 0$ is used in this type of analysis because:

- sliding resistance along the block–block interface is basically frictional when shear keys and/or connection pins are absent;
- the experimental result of $C_B = 5$–15 kN/m reported by Bathurst and Simac (1997) may be contributed by the shear keys or pins between the facing blocks. The effect of c_B induced by the shear strength of connecting pins will be discussed in Section 6.3.

For the case at site 4, $\phi_s = 48.1^\circ$ was used, which is larger than the values of 26–35° shown above. However, the difference between the calculated F_s values obtained by using $\phi_B = 48.1^\circ$ and $\phi_B = 26$–35° is negligible, because the length of the slip surface at the block–block interface is very small compared with the total length of the wedge failure planes in the backfill.

6.3. Type 3 analysis

In this analysis, the structural strength of the facing and the pull-out resistance of the reinforcement from the interface between the vertically adjacent blocks of facing are taken into account, as in the type 2 analysis, while considering the contribution of the strength of the connection pins placed between vertically adjacent facing blocks to the limit equilibrium stability along the failure planes. The values of T_w and T_s are obtained from Equations 4 and 5, as for the type 2 analysis. In this type of analysis, the contribution of the shear strength of the FRP connecting rods to the structural strength of the facing was represented by an equivalent cohesion intercept, $c_B = 47.3$ kN/m, which is obtained by multiplying the shear strength of a FRP rod with the total number of FRP rods per meter of the wall (= 4.5 in the present study).

Figures 20a–d show the relationships between the global safety factor, F_s, and the horizontal seismic coefficient, k_h, of the walls at sites 1–4 obtained by these three types of analysis. The critical failure mechanisms for the GRS-MB retaining walls at these sites were determined using a trial-and-error searching method. In these figures, ϕ_s is the internal friction angle of the backfill soil obtained from direct shear tests, as summarised in Table 1. The strengths (c_h and $\tan \phi_h$) along the horizontal soil–reinforcement interface and those along the base of the reinforced soil zone were reduced by a factor of 0.8 for all the cases investigated: that is, $c_h = 0.8c_s$ and $\tan \phi_h = 0.8 \tan \phi_s$. Despite the use of $c_h = 0.8c_s$ and $\tan \phi_h = 0.8 \tan \phi_s$, the sliding along the base of the reinforced zone or along the soil–reinforcement interface never controlled the failure of these walls; the failure along the bi-linear failure lines in the backfill was dominant, as shown in Figures 21a–d.

The critical horizontal seismic coefficient, k_{h_c} (or the critical horizontal yielding acceleration divided by the gravitational acceleration), is equal to the value of k_h when $F_s = 0$ along the respective curve of F_s against k_h presented in Figures 20a–d. The following trends of behaviour can be seen:

- For the GRS-MB retaining walls at sites 1, 2 and 3, the difference of k_{h_c} between the type 2 analysis (with connection strength between facing and backfill but without the shear strength of the FRP rod) and the type 1 analysis (without facing) ranges between 170% and 200%. For the GRS-MB retaining wall at site 4, however, the difference is only 19%. This result also suggests that, as the shear strength of the backfill soil increases, the effects of the structural strength of the facing on the global seismic stability of the whole wall system decreases, and could become very small when the shear strength of the backfill soil becomes very high, as is the case at site 4. Note that, even in this case, the seismic stability of the facing cannot be ensured when the connection strength is too low, resulting in the total collapse of the facing separating from the reinforced backfill. This type of failure mode is not allowed in most cases.
- For the GRS-MB retaining walls at sites 1, 2 and 3, the values of k_{h_c} obtained by the type 3 analysis (with connection strength together with the contribution of the shear strength of the FRP rod to the seismic stability of the wall) are significantly higher than the respective values obtained by the type 2 analysis. This result indicates a potentially high contribution of the FRP connection rods to the seismic stability of GRS-MB retaining walls. These results from type 1 and type 2 analysis, together with the results from type 3 analysis, indicate potential paramount effects of the structural strength of the facing together with the connection strength on the high seismic stability of reinforced soil-retaining walls.
- Sites 1–3 were located in a less seismically active area in Taiwan. The maximum design horizontal ground acceleration (a_{max}) was 230 gal, and a design value of $k_h = 0.115$ has been suggested for the design of earth-retaining structures for highway bridges (Ministry of Transport 1995). It can be seen from Figures 20a–b that the values of k_{h_c} for type 2 and 3 analyses are all greater than 0.115. The values of k_{h_c} are approximately equal to or larger than the design value of k_{h_c} used for the seismically active areas in Taiwan ($a_{max} = 330$ gal, design value of $k_h = 0.165$: this value is to be used in the new seismic design guidelines after the 1999 Chi-Chi earthquake) in Taiwan. Nevertheless, large displacements of the walls observed at sites 1 and 2 reveal the limitation of applying a pseudo-static approach in the seismic design of GRS-MB walls. To overcome this inherent drawback, displacement-based seismic design of GRS-MB walls is necessary.

The field investigation at the sites showed that the diameter of the slot in the modular blocks in which each

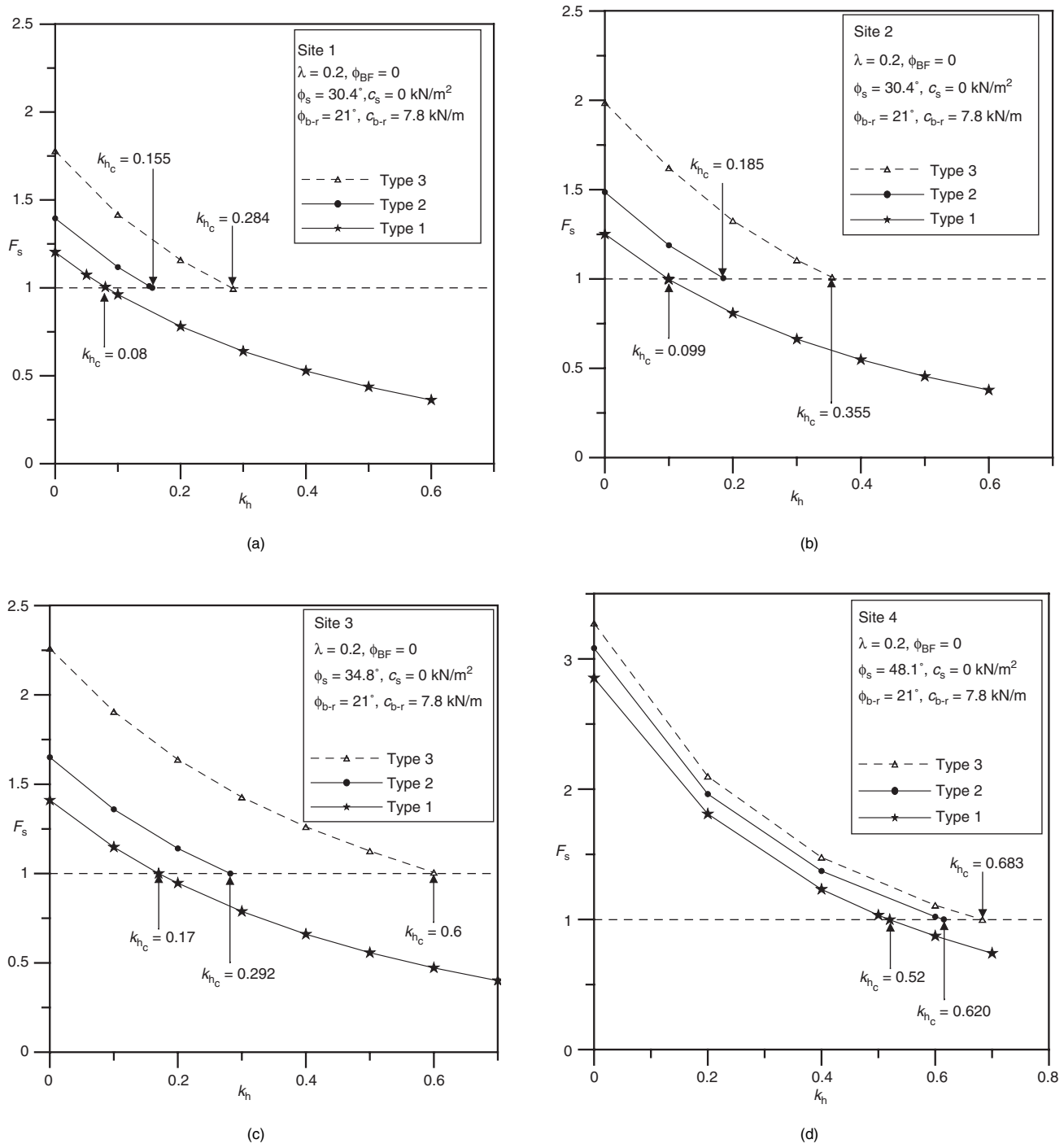

Figure 20. F_s–k_h relationships for GRS-MB walls at: (a) site 1; (b) site 2; (c) site 3; (d) site 4

FRP connection pin was inserted was much larger, by about 30 mm, than the diameter of the FRP connection pins, which was 13 mm. At the same time, the FRP connection rods observed at large openings between modular blocks (Figure 9) and the top and bottom surfaces of the modular blocks of the totally collapsed parts of the facing at sites 1 and 2 were intact. Based on the above and other observations, it is very likely that the full connection strength of the FRP rods was not activated with these failed GRS-MB retaining walls at sites 1 and 2, and this was one of the major causes of the failure of these walls. From this point of view, type 2 analysis may be more appropriate than type 3 for simulating the seismic behaviour of the GRS-MB walls at sites 1–4.

Based on the field observations and the presented results of the analysis, it seems that the possible scenario relevant to the failure of the GRS-MB retaining walls at sites 1 and 2 is as follows.

1. With a downward drag force along the back of the facing induced by the settlement of relatively loose backfill, buckling-mode deformation of the facing was triggered. Buckling deformation continued with

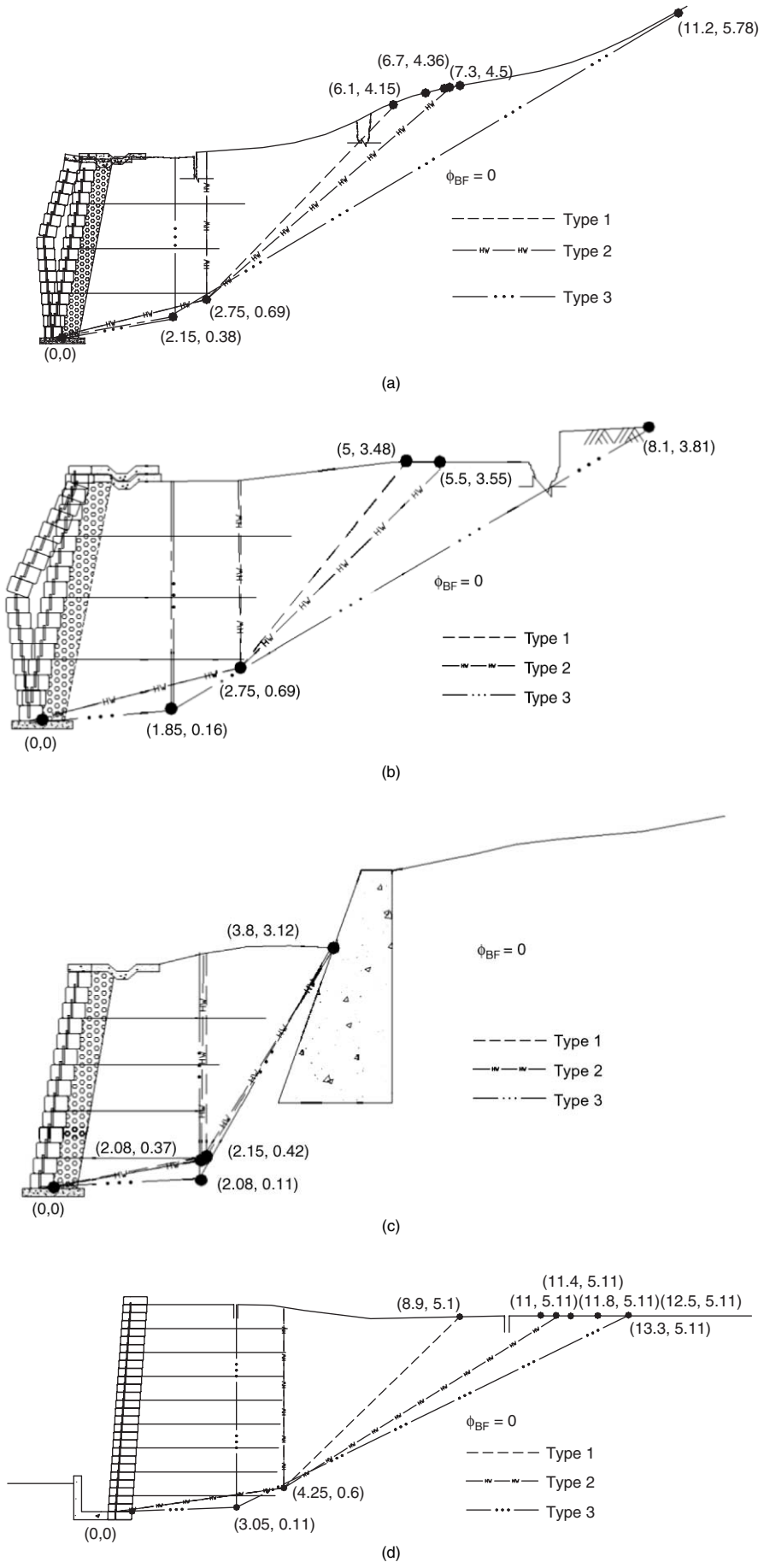

Figure 21. Critical failure surfaces obtained using various types of analysis for the GRS-MB walls at: (a) site 1; (b) site 2; (c) site 3. (d) Effects of facing and connecting force on the critical failure surface for the GRS-MB wall at site 4

increased seismic earth pressure against the wall and insufficient pull-out resistance of the geogrid from the block–block interface.

2. As the full rupture strength of the FRP connection rods could be mobilised only after the relative displacement between the vertically adjacent modular blocks became very large, large relative displacements between the vertically adjacent modular blocks took place without being restrained by the shear resistance of the FRP connection rods. Even when a relatively large force tended to act on the FRP connection rods, the junction of the geogrid at the pins would have ruptured, and then the geogrid was pulled out from the block–block interface because of a very low junction strength (Figure 8).
3. The buckling of the facing resulted in a large opening at the interface between vertically adjacent modular blocks, which in turn resulted in a total separation of the FRP connection rods from the vertically adjacent modular blocks (Figure 9). As a result, the shear resistance at the interface between the reinforcement and the vertically adjacent modular blocks was completely lost. This accelerated the deformation and displacement of the facing, resulting in the ultimate failure of the facing (Figure 10).

The lessons learnt from these case histories are therefore as follows.

The structural role of the facing in the stability of the wall under seismic loading conditions is evident. In addition to the horizontal seismic force against the facing, the downward drag force along the rear side of the facing should be properly accounted for. Not only the shear resistance between the individual modular blocks but also the bending resistance against possible buckling failure of the entire facing structure should be taken into account in the seismic design of GRS walls.

A sufficiently high connection strength, T_b, should be ensured by proper consideration of the following factors:

- the configurations of the connection pins, including the length, the fitness to the modular blocks, and the rupture strength of the pins;
- the junction strength of the geogrid at the locations of the pins;
- the shear resistance along the interface between the geogrid and the vertically adjacent modular blocks; and
- excessive outward displacement of the facing when buckling mode deformation is likely to occur.

If the connection strength is overestimated by ignoring these factors, the seismic stability of GRS-MB retaining walls is also overestimated.

7. DISPLACEMENT ANALYSIS USING MODIFIED TWO-WEDGE METHOD

Figures 22a and 22b show the displacement diagrams used for calculating the deformation and displacement of the facing and the backfill wedges. The main advantage of incorporating displacement diagrams in the displacement calculation is that both vertical and horizontal displacements of the backfill wedges behind the facing can be obtained. In particular, proper evaluation of the vertical settlement at the crest of the backfill during earthquakes is of practical significance when the wall crest is opened to traffic, such as highways and railways. This evaluation is not possible by the existing methods (e.g. Cai and Bathurst 1996; Ling and Leshchinsky 1998), in which only the horizontal displacement of the

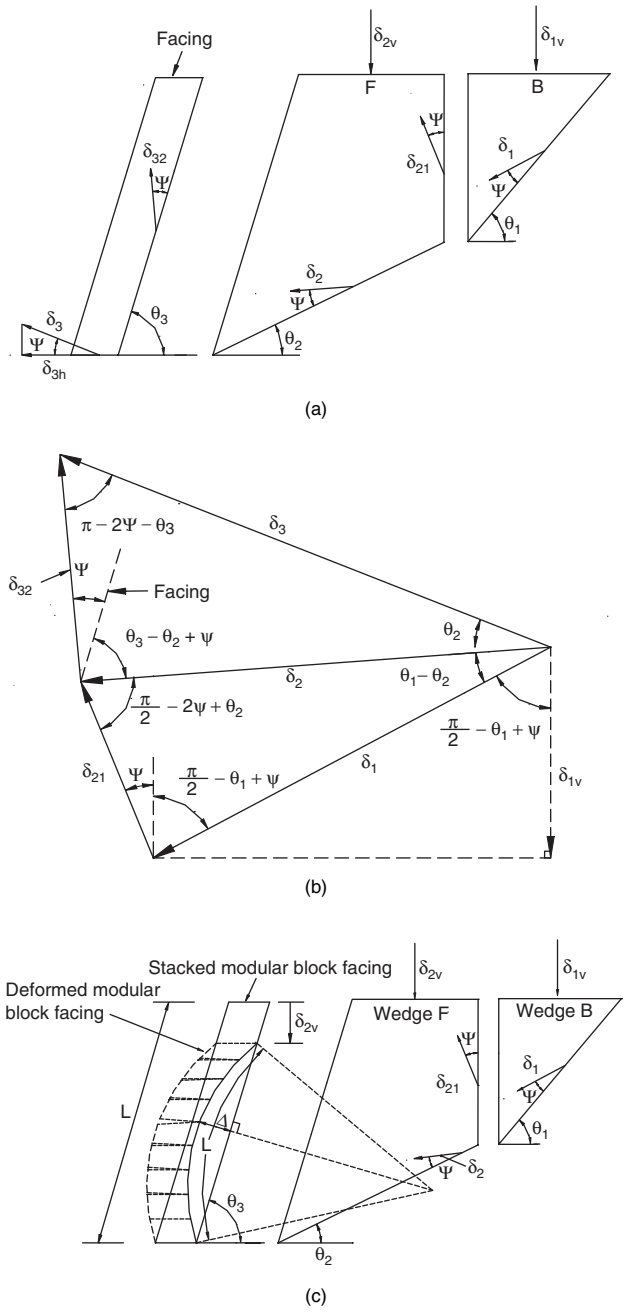

Figure 22. (a) Translational displacement mode of soil wedges and rigid panel facing under no restraint at the toe of facing; (b) displacement diagram based on the modified two-wedge method; (c) translational and buckling modes of displacement of soil wedges and dry-stacked modular block facing under restraint at toe of footing

reinforced backfill zone along the base of wall can be evaluated. The displacement diagrams shown in Figures 22a and 22b are similar to those used for the upper bound solution in the limit analysis (Atkinson 1981) except for the following point: the dilatancy angle, ψ, that controls the 'flow' along the failure planes at the interface between the backfill soil wedges and the surrounding stationary one is equal to the internal friction angle, ϕ_s, in the upper bound solution, whereas $\psi = 0$ is assumed in the present analysis, for the following reasons:

- With uncemented granular materials, the largest dilatancy angle, denoted as ϕ, is activated when the peak value of ϕ_s is mobilised, and the value of ψ is substantially smaller than the value of ϕ_s, usually by about 30° (e.g. Tatsuoka 1987; Tatsuoka *et al.* 1986).
- The angle of dilatancy decreases towards zero in the post-peak regime as the mobilised friction angle decreases from the peak value to the residual value after a limited amount of shear displacement is exhibited along the failure plane. A failure plane is actually a shear band having a thickness that is approximately 10–20 times the mean diameter of the soil (e.g. Yoshida and Tatsuoka 1997; Yoshida *et al.* 1995).

It was therefore considered that the assumption that $\psi = 0$ would be relevant in the analyses for sites 1 and 2 for their great displacements whereas the use of a non-zero, small value of ψ for sites 3 and 4 would be more realistic. More studies on the effect of ψ on the displacements of GRS walls are necessary.

In the present study, the following two modes of displacement of facing were considered in calculating the displacements of the walls.

7.1. Translational displacement of facing (Figure 22a)

This mode of displacement is typical for GRS walls with non-yielding full-height panel facings. The sliding block theory proposed by Newmark (1965), which is schematically explained in Figure 23, was used to calculate the horizontal component, δ_{3h}, of the displacement of the non-yielding rigid full-height panel facing, shown in Figure 22a. In the present calculation, the time history of horizontal ground acceleration in the relevant direction recorded at a nearby seismograph (TCU052) was used for the GRS-MB retaining walls at sites 1, 2 and 3. The displacement components other than δ_{3h} can then be calculated based on their geometrical relation, shown in Figure 22c. For example, the vertical settlement of soil wedge F can be calculated as

$$\delta_{2v} = \delta_{3h} \frac{\sin(\theta_2 - \psi)}{\cos\psi} \cdot \frac{\sin(2\psi + \theta_3)}{\sin(2\psi + \theta_3 - \theta_2)} \tag{6}$$

In the analysis of rigid full-weight panel facings, type 2 analysis was performed by assuming no buckling mode deformation of the facing.

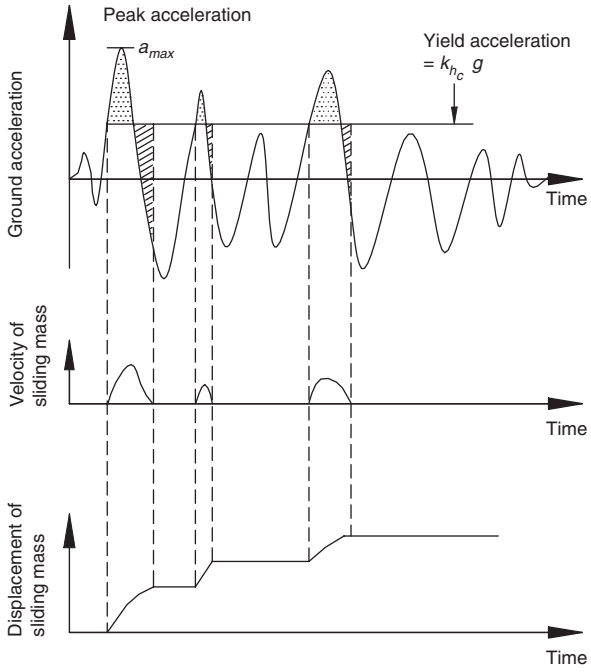

Figure 23. Schematic diagram for calculating seismic displacement of wall based on Newmark's theory

7.2. Buckling and translational displacement of facing (Figure 22c)

This mode of displacement is typical for the GRS walls with discrete modular block facing analysed in the present study. In this case, the horizontal displacement, δ_h, of the facing is expressed by

$$\delta_h = \delta_{2h} + \Delta_h \tag{7}$$

where δ_{2h} is the horizontal component of δ_2, which is the movement of the soil wedge F (Figure 22b), obtained by Newmark's sliding block theory using the relevant recorded time history of horizontal ground acceleration; and Δ_h is a component resulting from the buckling of the facing, which is obtained as

$$\Delta_h = \Delta \sin\theta_3 \tag{8}$$

where Δ is the maximum lateral deformation of the facing, obtained as

$$\Delta = \frac{3}{16}\sqrt{2\delta_{2v}\sec\theta_3(L - \delta_{2v}\sec\theta_3)} \tag{9}$$

which is obtained from the following equation (Miyamoto and Matsuda 1987):

$$L = \sqrt{(L - \delta_{2v}\sec\theta_3)^2 + \frac{16}{3}\Delta^2} \tag{10}$$

where L is the original length of the facing, and δ_{2v} is the vertical settlement of soil wedge F, which is assumed to be the same based on the observations at sites 1 and 2, as shown in Figures 6b and 7b. Equation 10 is utilised in the present study under the assumption that the deformed facing can be described by a segment of arc. Referring to Figure 22c, the value of δ_{2v} is obtained as

$$\delta_{2v} = \delta_{2h}\tan(\theta_2 - \psi) \tag{11}$$

A PC-based computer program was developed to calculate the F_s and k_h relationships and the critical horizontal seismic coefficient, k_{h_c}, for various facing and connection types. This program also calculates the displacements of the facing and the backfill (i.e. δ_h, δ_{3h} and δ_{2v}) for an input time history of ground acceleration and a known value of k_{h_c}.

Figure 24a shows the major part of the N–S component of the ground acceleration recorded at a station (TCUO52) that was near sites 1, 2 and 3 during the Chi-Chi earthquake. Also shown is the value of k_{h_c} that was obtained using the measured internal friction angle $\phi_s = 30.4$ (Table 1) and type 2 analysis for the GRS-MB retaining wall at site 1. The calculated horizontal displacements of the facing (δ_{3h} and δ_h) and vertical settlement of block F (δ_{2v}) for the severely deformed section at site 1 (see Figure 6b) are shown in Figure 24b. It may be seen that the proposed method (by type 2 analysis) gives the displacements δ_h (= 638 mm) of the yielding facing that are comparable to those observed in the field (≈470 mm). The value of δ_{2v} measured at the severely deformed section (≈100 mm) is also comparable to the calculated value (≈138 mm). It may also be seen that the displacement, δ_h, of the discrete block facing—that is, translation plus buckling—is larger than the value for the non-yielding facing (δ_{3h}) by about 14%.

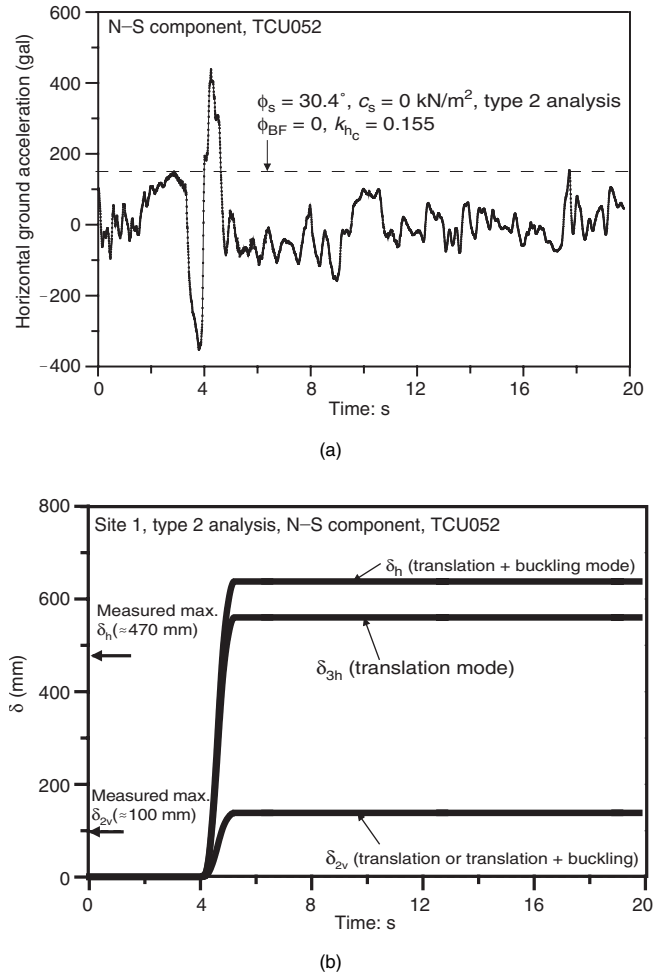

Figure 24. GRS-MB wall at site 1: (a) input ground acceleration and yield acceleration; (b) displacement–time relationships

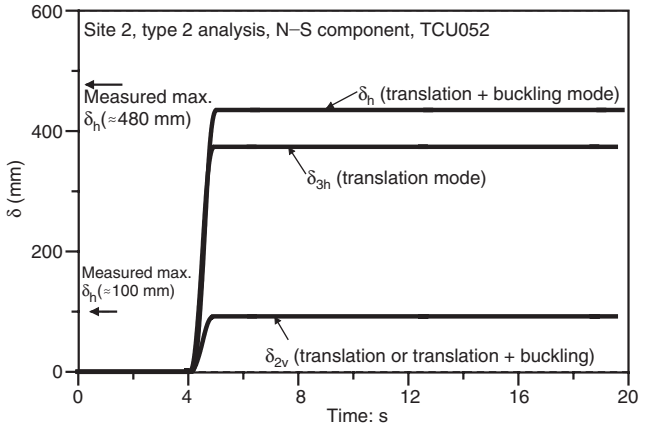

Figure 25. Displacement–time relationships for GRS-MB wall at site 2

Figure 25 shows the time histories of displacements for the severely deformed section (see Figure 7b) at site 2. It may be seen that the calculated value of δ_h (equal to 435 mm) for the yielding facing is comparable to the measured value (= 480 mm). Comparing the values of k_{h_c} for site 1 (= 0.158) and site 2 (= 0.185), variations of the k_{h_c} value of 17% and δ_h of about 32% (638 mm for site 1 and 435 mm for site 2) can be detected. However, the measured values of δ_h at sites 1 and 2 were fairly similar (470 mm for site 1 and 480 mm for site 2). These differences in the calculated values of k_{h_c} and δ_h reflect the effects of different geometries of the sloped backfill.

Figure 26 shows the time histories of displacements for the wall at site 3. The calculated value of δ_h (= 142 mm) of the yielding facing is only about 20–30% of those for the walls at sites 1 and 2. The calculated value of δ_h/H (= 142/2650 = 0.053) was therefore about 5%. It is likely that this relatively small deformation of the wall of this order was difficult to be detected at the site. It is possible that some minor cracks that were observed at the crest of the backfill and the facing modular block reflected this order of small wall deformation.

For the wall at site 4, the value of k_{h_c} calculated by type 2 analysis was as high as 0.615. This value is even

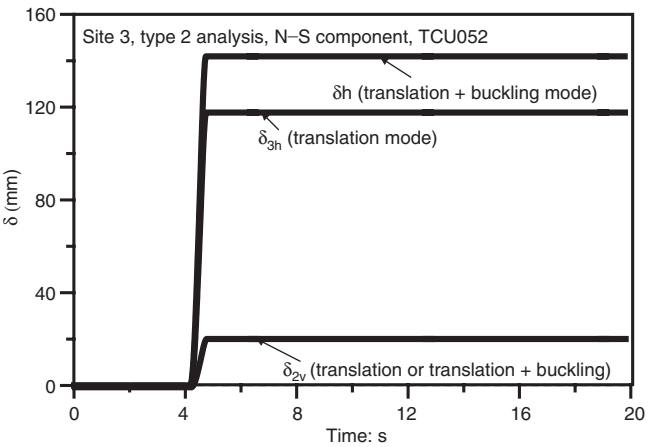

Figure 26. Displacement–time relationships for GRS-MB wall at site 3

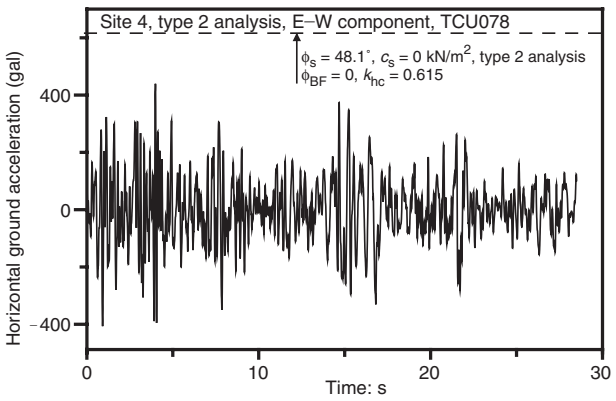

Figure 27. Input ground acceleration and yield acceleration of GRS-MB wall at site 4

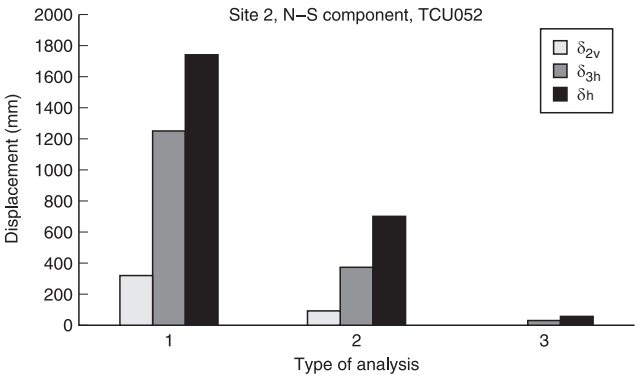

Figure 29. Residual seismic displacements of GRS-MB wall at site 2 using various types of analysis

greater than that of the value of a_{max}/g obtained from a nearby seismograph (see Figure 27). For this reason, the calculated values of δ_{3h} and δ_{2v} for this wall are zero. This result of the analysis is consistent with the observations in the field.

Figures 28–30 show the values of displacements (δ_{3h}, δ_h and δ_{2v}) for various types of analysis (types 1, 2 and 3) calculated with the same method as used to derive Figures 24b, 25 and 26. It can be seen that the displacements of GRS-MB walls that do not take into account the structural stabilising function of the facing (i.e. type 1) are significantly higher than those when the

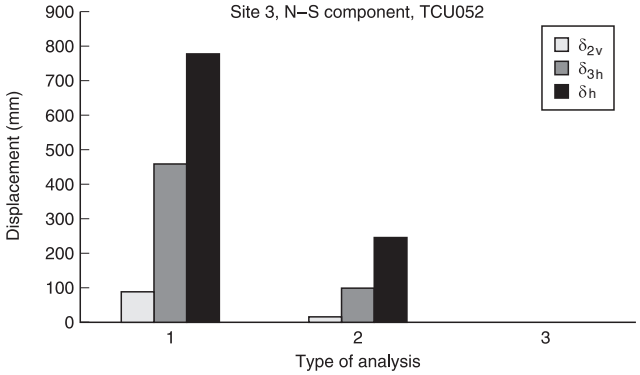

Figure 30. Residual seismic displacements of the GRS-MB wall at site 3 using various types of analysis

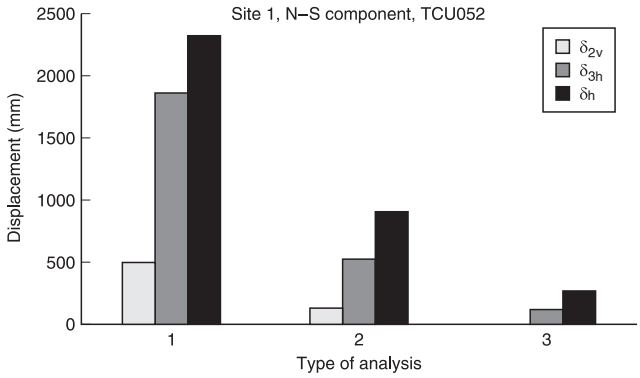

Figure 28. Final seismic displacements of GRS-MB wall at site 1 using various types of analysis

facing *is* taken into account (i.e. types 2 and 3). It is also seen in Figures 28–30 that the displacements calculated using type 3 analysis are significantly smaller than those obtained using type 2 analysis, possibly as a result of overestimation of the structural effect of the FRP rods used for connecting the modular blocks.

Table 3 compares the measured values of δ_h and δ_{2v} for sites 1–4 with those calculated using type 2 analysis. In this table the values 'Calc. R_1', defined as the ratio between the calculated δ_h and the calculated δ_{3h}, are shown. It can be seen that the values of Calc. R_1 ranged between 1.14 and 1.206 for sites 1–3. It has been shown previously that a larger horizontal displacement for the

Table 3. Seismic displacements of facings and backfill

Site	Calc. δ_{3h} (mm)	Calc. δ_h (mm)	Calc. δ_{2v} (mm)	Calc. R_1[(a)]	Calc. R_2[(b)]	Meas. δ_h (mm)	Meas. δ_{2v} (mm)	Meas. R_2[(c)]
1	559	638	138	1.140	0.249	470	100	0.212
2	374	435	92	1.164	0.247	480	100	0.208
3	118	142	21	1.206	0.178	0	0	–
4	0	0	0	–	–	0	0	–

[(a)] Calc. $R_1 = \dfrac{\text{calculated}\delta_h}{\text{calculated}\delta_{3h}}$.

[(b)] Calc. $R_2 = \dfrac{\text{calculated}\delta_{2v}}{\text{calculated}\delta_h}$.

[(c)] Meas. $R_2 = \dfrac{\text{measured}\delta_{2v}}{\text{measured}\delta_h}$.

stacked block facing resulted from the buckling mode of the stacked block facing. It is also seen in Table 3 that the calculated values of Calc. R_2 ($= \delta_{2v}/\delta_h$) range between 0.247 and 0.249. These values are comparable with the measured ones (i.e. Meas. $R_2 = 0.212$ and Meas. $R_2 = 0.208$ for the severely deformed sections at site 1 and site 2, as shown in Figures 6b and 7b, respectively).

8. CONCLUSIONS

Four geosynthetic-reinforced soil modular block (GRS-MB) retaining walls that behaved very differently during the 1999 Taiwan Chi-Chi earthquake were investigated, including subsurface explorations at the sites and laboratory shear tests of the backfill materials. A modified two-wedge method was developed to evaluate the safety factor as well as deformation and displacement of the walls subjected to seismic load for possible different failure modes, such as external and internal horizontal sliding of the reinforced backfill. The characteristic features of this method are that the structural effects of facing and the connection strength between the reinforcement and the facing are taken into account. The seismic displacements of the facing and the settlement of the backfill soil wedge can be evaluated by taking into account the displacement compatibility between the facing structure and the backfill soil wedges.

The following was found from the present study:

- Failures and/or large deformations of the GRS-MB walls at sites 1 and 2 may result from a combined effect of the seismic earth thrust induced by strong ground accelerations, a downward drag force along the back of the block facing caused by the high deformability of relatively loose backfill, insufficient reinforcement-to-facing anchorage strength, and insufficient lateral confinement for the soil induced by the geogrids. The latter two factors can be closely related to the overly large vertical spacings of the geogrids.
- The modified two-wedge failure mechanism may explain the buckling mode deformation of the facing at sites 1 and 2 based on the concept of displacement compatibility between the facing and the soil wedges, and the pseudo-static analyses using the modified two-wedge failure mechanism result in critical failure lines in good agreement with the observed open cracks at site 1.
- A method for evaluating the deformation and displacement of reinforced soil-retaining walls based on the modified two-wedge failure mechanism was developed by extending Newmark's sliding block theory, incorporating the displacement diagrams as used for the upper bound solution. It was found that both the seismic stability and the seismic displacements of the GRS-MB walls at sites 1–3 were strongly affected by the geogrid-to-facing connection strength and the shear strength at the block–block interface.
- The conventional two-wedge method, which does not take into account the structural effects of the facing and the connection strength, may considerably underestimate the seismic stability of reinforced soil-retaining walls with facing rigidity and connection strength. The extent of the underestimate is a function of the strength of the backfill soil. When a relatively loose backfill is used, the underestimation of the value of k_{h_c} could be very significant.
- The type 3 analysis, considering full mobilisation of the shear resistance at the block–block interface, overestimates the seismic stability of the wall to a large extent. Some factors that have a critical effect on mobilisation of the shear resistance of the connecting rods, such as the fit of the rod in the slot and the structural integrity of the modular block facing, should not be overlooked.
- A disagreement was found between the results of limit-equilibrium-based analyses and the displacements observed for the GRS-MB walls at sites 1 and 2. The analytical values of k_{h_c} calculated for these sites indicated that these walls fulfilled seismic design requirements in Taiwan. Nevertheless, they exhibited severe displacement (or collapse) of the facings and retained soils, indicating that a displacement-based design of GRS-MB walls against strong earthquakes is necessary.
- The deformation and displacement of the investigated walls calculated by the proposed method using type 2 analysis (that is, the geogrid-to-facing connection strength was considered, but the shear strength of the FRP rods was not considered) were comparable to the observed values, allowing for some discrepancy due perhaps to the approximate nature of the input soil parameters and the proposed method.
- The horizontal displacements of the modular block facing considering buckling mode deformation is 14–16% larger than that for a rigid facing wall. This assumes that the calculated values of k_{h_c} for rigid and modular block facings are equal. Therefore the difference could be even larger when the internal shear strength of the facing structure and geogrid-to-facing connection strength are taken into account.

ACKNOWLEDGEMENTS

The present study was financially supported by the National Science Council, Taiwan, under contract no. NSC 89-2218-E-006-144. The authors acknowledge the financial and technical support from Dr M. Tateyama, Railway Technical Research Institute, Japan, Dr Y. Iwasaki, Director of Geo-Research Institute, Japan, and Dr O. Matsuo, Head of Soil Dynamic Division, Public Works Research Institute, Ministry of Construction, Japan, in the post-earthquake investigation of the 1999 Taiwan Chi-Chi earthquake. Detailed information on the investigated GRS-MB walls provided by the Second Construction Divisions of the Taiwan Public Highway Bureau and by the Taiwan Residential Housing and Urban Development Bureau is also acknowledged.

APPENDIX A

The inter-wedge force P_{BF} is derived as follows from the force equilibrium in the horizontal (X) and vertical (Y) directions for wedge B (see Figure 17):

$$P_{BF} = \frac{\left\{\begin{array}{l}(Q_{BV} + C_{BF})\tan(\theta_1 - \phi_S) \\ \quad + W_B[(1 - k_v)\tan(\theta_1 - \phi_S) + k_h] \\ \quad + Q_{BH} - C_B[\cos\theta_1 + \sin\theta_1 \tan(\theta_1 - \phi_S)]\end{array}\right\}}{\cos\phi_{BF} + \sin\phi_{BF}\tan(\theta_1 - \phi_S)} \tag{8}$$

where Q_{BV} and Q_{BH} are the vertical and horizontal loads, respectively, acting on the top of wedge B; C_{BF} is the cohesive shear resistance between wedges B and F; ϕ_{BF} is the friction angle acting along the interface between wedges B and F; W_B is the self-weight of wedge B; k_v and k_h are the vertical and horizontal seismic coefficients, respectively; and T_{BF} and T_B are the tensile forces (positive) in the reinforcement acting at the interface between B and F and at the bottom of wedge B, respectively.

From the force equilibrium in the X and Y directions, the interface force between the facing and wedge F, P_F, can be derived as

$$P_F = \frac{\left\{\begin{array}{l}Q_{FH} + P_{BF}[\cos\phi_{BF} - \sin\phi_{BF}\tan(\phi_S - \theta_2)] \\ \quad - [Q_{FV} + C_{BF} + (1 - k_v)W_F]\tan(\phi_S - \theta_2) \\ \quad - C_{FW}[\cos\theta_3 + \sin\theta_3 \tan(\phi_S - \theta_2)] \\ \quad - C_F[\cos\theta_2 - \sin\theta_2 \tan(\phi_S - \theta_2)]\end{array}\right\}}{\left\{\begin{array}{l}\cos\left(\phi_{FW} + \theta_3 - \frac{\pi}{2}\right) \\ \quad + \sin\left(\phi_{FW} + \theta_3 - \frac{\pi}{2}\right)\tan(\theta_2 - \phi_S)\end{array}\right\}} \tag{9}$$

where Q_{FV} and Q_{FH} are the vertical and horizontal loads, respectively, acting on the top of wedge F; T_F and T_{BF} are the tensile reinforcement force acting at the bottom of wedge F and at the interface between wedges B and F, respectively; T_W is the connection force acting at the interface between the facing and wedge F; C_F is the cohesive shear resistance acting at the bottom of wedge F; and W_F is the self-weight of wedge F.

Based on the force equilibrium in the X and Y directions for the modular block facing (or soil-retaining wall), consider a virtual force, P_{EX}, acting in the X direction to maintain the equilibrium condition. P_{EX}, can be expressed as follows:

$$\begin{aligned} P_{EX} = & -P_P + Q_{WH} - C_W + k_h W_W - T_W \cos\beta \\ & + P_F \cos\left(\phi_{FW} + \theta_3 - \frac{\pi}{2}\right) \\ & - \left[Q_{WV} + (1 - k_v)W_W + C_{FW}\sin\theta_3 \right. \\ & \left. + P_F \sin\left(\phi_{FW} + \theta_3 - \frac{\pi}{2}\right) + T_W \sin\beta\right]\tan\phi_W \\ & + C_{FW}\cos\theta_3 \end{aligned} \tag{10}$$

where Q_{WV} and Q_{WH} are the vertical and horizontal loads, respectively, on the top of the facing; P_P is the passive resistance acting at the bottom of the facing; C_{FW} and C_W are the cohesive shear resistances acting along the interface between the facing and wedge F and at the bottom of wedge W, respectively; and W_W is the self-weight of the facing.

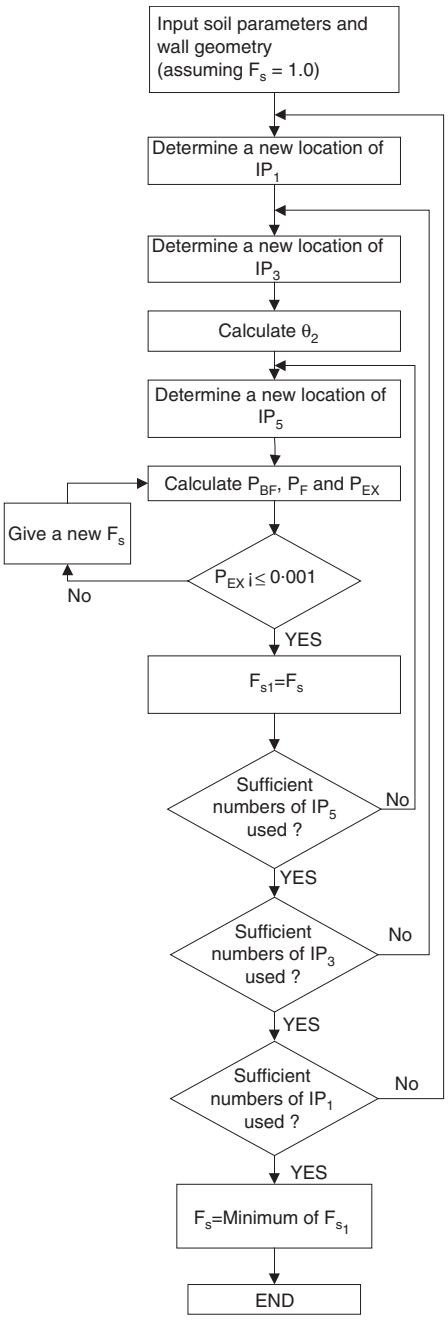

Figure 31. Flow chart for the computer program used to evaluate seismic stability of GRS-MB walls

Figure 31 shows the flowchart for the computer program 'SD-RMBW' developed to calculate the minimum value of F_s and seismic displacements for a wall when using the seismic coefficient k_h and λ ($= k_v/k_h$).

NOTATIONS

Basic SI units are given in parentheses.

a_{max} peak ground acceleration (gal)
B base width of facing (m)

c_B cohesive resistance at block-to-block interface (N/m)
c_{BF} inter-wedge cohesion intercept (N/m^2)
C_{BF} cohesive resistance at inter-wedge failure plane (N/m)
$C_{b\text{-}r}$ cohesive resistance of geogrid-to-block interface (N/m)
C_F cohesive resistance at base of wedge F (N/m)
c_{FW} cohesion intercept along facing-to-backfill interface (N/m^2)
C_{FW} cohesive resistance at facing-to-backfill interface (N/m)
c_h cohesion intercepts for horizontal soil-geogrid interface and for base of reinforced soil zone (N/m^2)
c_s cohesion intercept of backfill soil (N/m^2)
C_W cohesive resistance at base of block facing (N/m)
F_s safety factor against shear failure of soil
g gravitational constant (= 980 gal)
H height of wall facing (m)
IP_i (i = 1–5) points controlling geometry of soil wedges (dimensionless)
K_{AE} seismic earth pressure coefficient (dimensionless)
k_h horizontal seismic coefficient (dimensionless)
k_{h_c} critical horizontal seismic coefficient (dimensionless)
k_v vertical seismic coefficient (dimensionless)
L embedment length of geogrid (m)
M_L Richter local magnitude (dimensionless)
M_w moment magnitude (dimensionless)
P_{BF} frictional inter-wedge force between wedges B and F (N/m)
P_{EX} horizontal virtual force applied at outside of facing (N/m)
P_F resultant force acting at back of facing (N/m)
P_n normal load on block–block interface (N/m^2)
P_P external force applied at toe of facing (N/m)
Q_{BV} Vertical load at the top of wedge B (N/m)
Q_{BH} horizontal load at top of wedge B (N/m)
Q_{FH} horizontal load applied at top of wedge F (N/m)
Q_{FV} vertical load applied at top of wedge F (N/m)
Q_{WH} horizontal load applied at the top of facing (N/m)
Q_{WV} vertical load applied at top of facing (N/m)
R_B frictional reaction force at base of wedge B (N/m)
R_F frictional reaction force at base of wedge F (N/m)
R_w frictional reaction force at base of block facing (N/m)
T_B reinforcement force acting at base of wedge B (N/m)
T_b pull-out resistance of geogrid from block–block interface (N/m)
T_{BF} reinforcement force acting at inter-wedge failure plane (N/m)
T_F reinforcement force acting at base of wedge F (N/m)
T_j junction strength of geogrid (N/junction)
T_{p_b} pull-out resistance of geogrid from soil behind failure surface (N/m)
T_{p_f} pull-out resistance of geogrid from soil in front of failure surface (N/m)
T_s mobilised reinforcement force at failure plane (N/m)
T_{ult} ultimate tensile strength of geogrids (N/m)
W_B self-weight of soil wedge B (N/m)
W_F self-weight of soil wedge F (N/m)
W_W self-weight of modular block facing (N/m)
β dip angle of reinforcement (degrees)
δ_1, δ_2, δ_3 displacements of wedge B, wedge F, and facing, respectively (m)
δ_{21} relative displacement between wedges B and F (m)
δ_{32} relative displacement between wedge F and facing (m)
δ_h horizontal displacement of yielding block facing (m)
δ_{2h} horizontal component of δ_2 (m)
δ_{3h} horizontal component of δ_3 (m)
δ_{1v} vertical component of δ_1 (m)
δ_{2v} vertical component of δ_2 (m)
Δ distance between deformed facing (assumed as an arc) and chord (m)
Δ_h horizontal component of Δ (m)
θ_1, θ_2, θ_3 Slope angles of facing, base of wedge F, and base of wedge B, respectively (degrees)
λ vertical-to-horizontal ratio of seismic coefficient (dimensionless)
τ_b geogrid-to-modular block bonding strength (N/m)
τ_f ultimate shear strength of backfill soil (N/m^2)
τ_m shear stress acting on failure plane (N/m^2)
τ_{p1}, τ_{p2} geogrid-to-soil bonding strength for various soil zones (N/m^2)
ϕ_B friction angle at block-to-block interface (degrees)
ϕ_{BF} friction angle between wedges B and F (degrees)
$\phi_{b\text{-}r}$ friction angle at geogrid-to-block interface (degrees)
ϕ_{FW} friction angle along facing-to-backfill interface (degrees)
ϕ_h friction angles at horizontal soil–reinforcement interface and at base of reinforced soil zone (degrees)
ϕ_{res} residual friction angle of backfill soil (degrees)
ϕ_s peak internal friction angle of backfill soil (degrees)
ϕ_w friction angle at base of block facing (degrees)
ψ angle of dilation of soil (degrees)

REFERENCES

Atkinson, J. H. (1981). *Foundations and Slopes: An Introduction to Applications of Critical State Soil Mechanics*, McGraw-Hill, London.

Bathurst, R. J. (1998). *Segmental Retaining Walls: Seismic Design Manual*, 1st edn, National Concrete Masonry Association, Herndon, VA, pp. 187.

Bathurst, R. J. & Hatami, K. (1998). Seismic response analysis of a geosynthetic-reinforced soil-retaining wall. *Geosynthetics International*, **5**, Nos. 1–2, 127–166.

Bathurst, R. J. & Simac, M. R. (1997). Design and performance of the facing column for geosynthetic reinforced segmental retaining walls. *Mechanically Stabilized Backfill*, Wu, J. T. H., Editor, Balkema, Rotterdam, pp. 193–208.

Bathurst, R. J., Cai, Z., Alfaro, M. & Pelletier, M. (1997). Seismic design issues for geosynthetic reinforced segmental retaining walls. *Mechanically Stabilized Backfill*, Wu, J. T. H., Editor, Balkema, Rotterdam, pp. 79–97.

Cai, Z. & Bathurst, R. J. (1996). Seismic-induced permanent displacement of geosynthetic-reinforced segmental retaining walls. *Canadian Geotechnical Journal*, **33**, 937–955.

Carotti, A. & Rimoldi, P. (1998). A nonlinear model for the seismic response analysis of geosynthetic-reinforced soil structures. *Geosynthetics International*, **5**, Nos. 1–2, 167–201.

Collin, J. G., Editor (1996). *Design Manual for Segmental Retaining Walls*, 2nd edn, National Concrete Masonry Association, Herndon, VA, pp. 65–67.

Horii, K., Kishida, H., Tateyama, M. & Tatsuoka, F. (1994). Computerized design method for geosynthetic-reinforced soil-retaining walls for railway embankments. *Proceedings of the International Symposium on Recent Case Histories of Permanent Geosynthetic-Reinforced Soil Retaining Walls*, Tatsuoka, F. and Leshchinsky, D., Editors, Balkema, pp. 205–218.

Huang, C. C. (2000). Investigations of soil-retaining structures damaged during the Chi-Chi (Taiwan) earthquake. *Journal of the Chinese Institute of Engineers*, **23**, No. 4, 417–428.

Huang, C. C., Chen, Y. H., Tateyama, M. & Tatsuoka, F. (2000). Increasing seismic stability of soil-retaining walls using soil reinforcing techniques. *Proceedings of the International Workshop on Annual Commemoration of Chi-Chi Earthquake, Sept. 2000, Taipei*, Loh, C. H. and Liao, W. I., Editors, Chinese Institute of Engineers, Taipei, pp. 229–240.

Huang, C. C., Chou, L. H. & Chen, Y. H. (2001). Analyses of a near-fault geosynthetic-reinforced modular block wall damaged during the 1999 Chi-Chi earthquake. *Proceedings of the International Symposium on Earth Reinforcement*, Ochiai *et al.*, Editors, Balkema, pp. 369–374.

Japanese Geotechnical Society (1988). *Methods of Ground Exploration*, Japanese Geotechnical Society, Tokyo, pp. 205–206 (in Japanese).

Japanese Railway Technical Research Institute (1999). *Design Guidelines for Railway Structures: Seismic Design*, Maruzen, Tokyo, pp. 317–329 (in Japanese).

Jewell, R. A., Paine, N. & Woods, R. I. (1984). Design methods for steep reinforced embankments. *Proceedings of the Symposium on Polymer Grid Reinforcement in Civil Engineering*, Thomas Telford, London, pp. 70–81.

Koseki, J., Munaf, Y., Tatsuoka, F., Tateyama, M. & Kojima, K. (1997). Shaking table and tilting tests of geosynthetic-reinforced soil-retaining wall and conventional type retaining wall models. *Geosynthetics International*, **5**, Nos. 1–2, 73–96.

Kotake, N., Tatsuoka, F., Tanaka, T., Siddiquee, M. S. A. & Huang, C. C. (2002). FEM simulation of the bearing capacity of level reinforced ground subjected to footing load. *Geosynthetics International*, **8**, No. 6, 501–549.

Ling, H. I. & Leshchinsky, D. (1998). Effects of vertical acceleration on seismic design of geosynthetic-reinforced soil structures. *Géotechnique*, **48**, No. 3, 347–373.

Matsuo, O., Tsutsumi, T., Yokoyama, K. & Saito, Y. (1998). Shaking table tests and analyses of geosynthetic-reinforced soil-retaining walls. *Geosynthetics International*, **5**, Nos. 1–2, 97–126.

Ministry of Transport, R.O.C (1995). *Manual of Traffic Technology: Traffic Engineering, Seismic Design of Highway Bridges*, Yu-Shy Publication Co., Taipei, pp. 34, 80 (in Chinese).

Miyamoto, T. & Matsuda, N. (1987). *Fundamental Mathematics Handbook*, Morihoku Publication Co., Tokyo, p. 158 (in Japanese, translated from Russian).

Mononobe, N. (1924). Investigations on vertical ground motion and some related topics. *Proceedings of the Civil Engineering Society, Japan*, **10**, No. 5, 1063–1094 (in Japanese).

Newmark, N. M. (1965). Effect of earthquakes on dams and embankments. *Géotechnique*, **15**, No. 2, 139–159.

Okabe, S. (1924). General theory on earth pressure and seismic stability of retaining wall and dam. *Proceedings of the Society of Civil Engineering, Japan*, **10**, No. 6, 1277–1323.

Schmertmann, G. R., Chouery-Curtis, V. E., Johnson, R. D. & Bonaparte, R. (1987). Design charts for geogrid-reinforced soil slopes. *Proceedings of the Geosynthetic 87 Conference*, New Orleans, pp. 108–120.

Seed, H. B. & Whitman, R. V. (1970). Design of earth retaining structures for dynamic loads. *Lateral Stresses in the Ground and Design of Earth Retaining Structures*, ASCE, pp. 103–147.

Siddiquee, M. S. A., Tanaka, T., Tatsuoka, F., Tani, K. & Morimoto, T. (1999). FEM simulation of scale effect in bearing capacity of strip footing on sand. *Soils and Foundations*, **39**, No. 4, 91–109.

Tatsuoka, F. (1987). Discussion on the paper by Bolton. *Géotechnique*, **37**, No. 2, 219–226.

Tatsuoka, F. (1993). Roles of facing rigidity in soil reinforcing. Keynote Lecture, *Proceedings of the International Symposium on Earth Reinforcement Practice*, IS Kyushu '92, Ochiai *et al.* (eds), Balkema, Rotterdam, **2**, 831–870.

Tatsuoka, F. & Yamauchi, H. (1986). A reinforcing method for steep clay slopes using a non-woven geotextile. *Geotextiles and Geomembranes*, **4**, 241–268.

Tatsuoka, F., Koseki, J., Tateyama, M., Munaf, Y. & Horii, K. (1998). Seismic stability against high seismic loads of geosynthetic-reinforced soil retaining structures. Keynote Lecture, *Proceedings of the 6th International Conference on Geosynthetics*, Atlanta, GA, pp. 103–142.

Tatsuoka, F., Sakamoto, M., Kawamura, T. & Fukushima, S. (1986). Strength and deformation characteristics of sand in plane strain compression at extremely low pressures. *Soils and Foundations*, **26**, No. 1, 65–84.

Tatsuoka, F., Tateyama, M. & Murata, O. (1989). Earth retaining wall with a short geotextile and a rigid facing. *Proceedings of the 12th International Conference on Soil Mechanics and Foundation Engineering*, Rio de Janeiro, **2**, 1311–1314.

Tatsuoka, F., Tateyama, M., Tamura, Y. & Yamauchi, H. (2000). Lessons from the failure of full-scale models and recent geosynthetic-reinforced soil-retaining walls. *Proceedings of the 2nd Asian Geosynthetics Conference, GeoAsia 2000*, Kuala Lumpur, **1**, 23–53.

Tatsuoka, F., Tateyama, M., Uchimura, T. & Koseki, J. (1997). Geosynthetic-reinforced soil-retaining walls as important permanent structures, 1996–1997 Mercer Lecture. *Geosynthetics International*, **4**, No. 2, 81–136.

University of Wisconsin-Platteville (1993). Evaluation of connection strength of keystone retaining wall units and Mirafi geogrids, test report, 3 August 1993.

Yoshida, T. & Tatsuoka, F. (1997). Deformation property of shear band in sand subjected to plane strain compression and its relation to particle characteristics. *Proceedings of the 14th International Conference on Soil Mechanics and Foundation Engineering*, Hamburg, **1**, 237–240.

Yoshida, T., Tatsuoka, F., Siddiquee, M. S. A. & Kamegai, Y. (1995). Shear banding in sands observed in plane strain compression. *Localisation and Bifurcation Theory for Soils and Rocks*, Chambon *et al.*, eds., Balkema, Rotterdam, pp. 165–179.

The Editors welcome discussion on all papers published in Geosynthetics International. Please email your contribution to discussion@geosynthetics-international.com by 15 August 2004.